

Pronounced Effect of pn-Junction Dimensionality on Tunnel Switch Sharpness

Sapan Agarwal and Eli Yablonovitch

Electrical Engineering & Computer Sciences Dept.

University of California, Berkeley, California, 94720

Abstract

Tunneling based field effect transistors (TFET's) have the potential for very sharp On/Off transitions if they exploit a sharp step in the density of states for switching. The same principle applies in Backward Diodes. As is well-known, the nature of the quantum density of states, is strongly dependent on dimensionality. Hence we need to specify both the n-side and the p-side dimensionality of pn junctions. For instance, we find that a typical bulk 3d-3d tunneling pn junction has only a quadratic turn-on function, while a pn junction consisting of two overlapping quantum wells (2d-2d) would have the preferred step function response. Quantum confinement on each side of a pn junction has the added benefit of significantly increasing the on-state tunnel conductance at the turn-on threshold. We find that there are nine physically distinguishable possibilities, 3d-3d, 2d-3d, 2d-2d, etc. Thus we introduce the obligation of specifying the dimensionality on either side of pn junctions.

Pronounced Effect of pn-Junction Dimensionality on Tunnel Switch Sharpness

Sapan Agarwal and Eli Yablonovitch

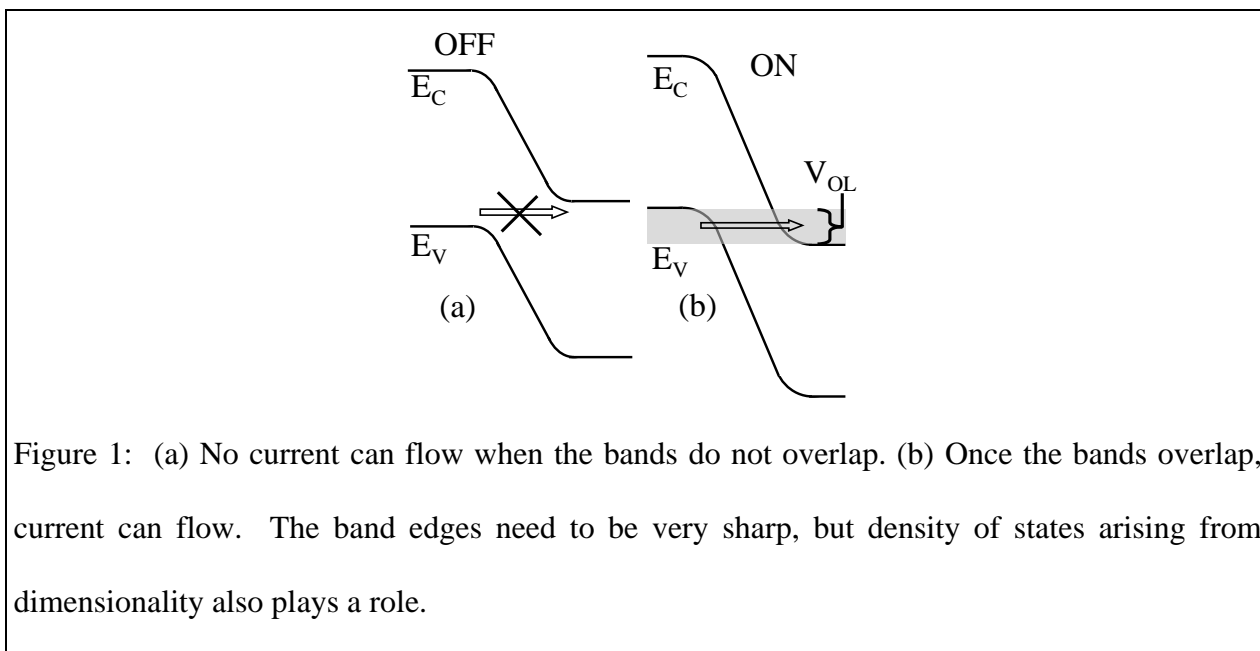
Table of Contents:

Abstract.....	1
Table of Contents:.....	2
II. 1d-1d Point Junction	5
III. 3d-3d Bulk Junction.....	8
IV. 2d-2d Edge Junction	10
V. 0d-1d Junction.....	11
VI. 2d-3d Junction	14
VII. 1d-2d Junction	17
VIII. 0d-0d Quantum Dot Tunneling.....	18
IX. 2d-2d Face Overlap	22
X. 1d-1d Edge Overlap	25
XI. Perturbation Tunnel Transmission Limit.....	27
XII. Maximum Conductance Limit	30
XIII. Smearing the Steep Response:	32
XIV. Density of States Broadening	35
XV. Conclusions.....	35
XVI. Acknowledgment.....	36
Appendix A: Transfer-Matrix Element Derivation	38
Appendix B: Using the Transfer Matrix Element to Derive Current	42
REFERENCES:	45

I. Introduction

Power consumption is increasingly critical for modern electronics. In the past, transistor voltage reduced with shrinking size, but in recent years the voltage scaling has stopped. At the end of the transistor roadmap¹, the operating voltage is projected to be 0.6V. Since transistors rely on the thermal excitation of carriers over an energy barrier, the Boltzmann factor makes it difficult to reduce the operating voltage much below this, while maintaining a good On/Off ratio. To further reduce the operating voltage, we need to change to a more sensitive switching mechanism. The family of Tunneling Field Effect Transistors (TFETs) includes a number of different mechanisms that may be promising for low voltage operation.

When trying to achieve a very sharp TFET turn on there are at least two mechanisms that can be exploited. The gate voltage can be used to modulate the tunneling barrier thickness and thus the tunneling probability^{2,3,4,5}. It is also possible use the band overlap or density of states threshold function. The band overlap turn-on is illustrated in Fig. 1. If the conduction and valence band do not overlap, no current can flow. Once they do overlap, there is a path for



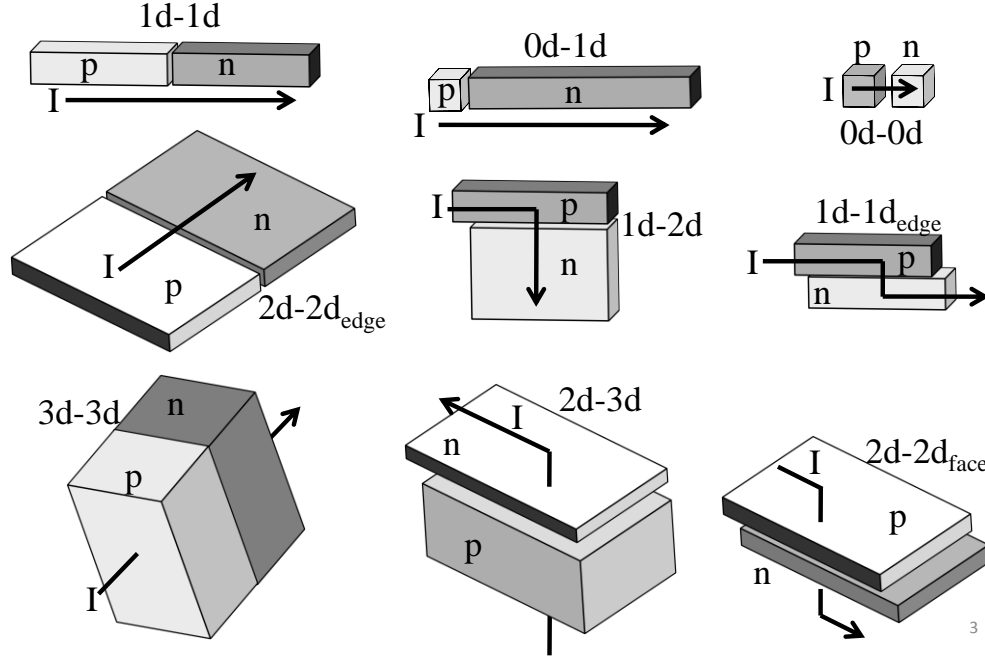


Fig. 2: We identify here the nine distinct dimensionality possibilities that we believe can exist in pn junctions. Each of the different tunneling pn junction dimensionalities shown have different turn on characteristics.

current to flow. This band overlap turn-on has the potential for a very sharp On/Off transition that is much sharper than that which can be achieved by modulating the tunneling barrier height or thickness⁶. If the band edges are ideal, one might expect an infinitely sharp turn on when the band edges overlap. We will find that in a typical 3d-3d bulk pn junction, the nature of the turn on is only quadratic in the control voltage. A sharper density-of-states occurs if the dimensionality on either side of the pn junction is reduced. In specifying a pn junction it is also necessary to specify the dimensionalities of p, and of n regions. We count nine different possible pn junction dimensional combinations, as shown in Fig. 2.

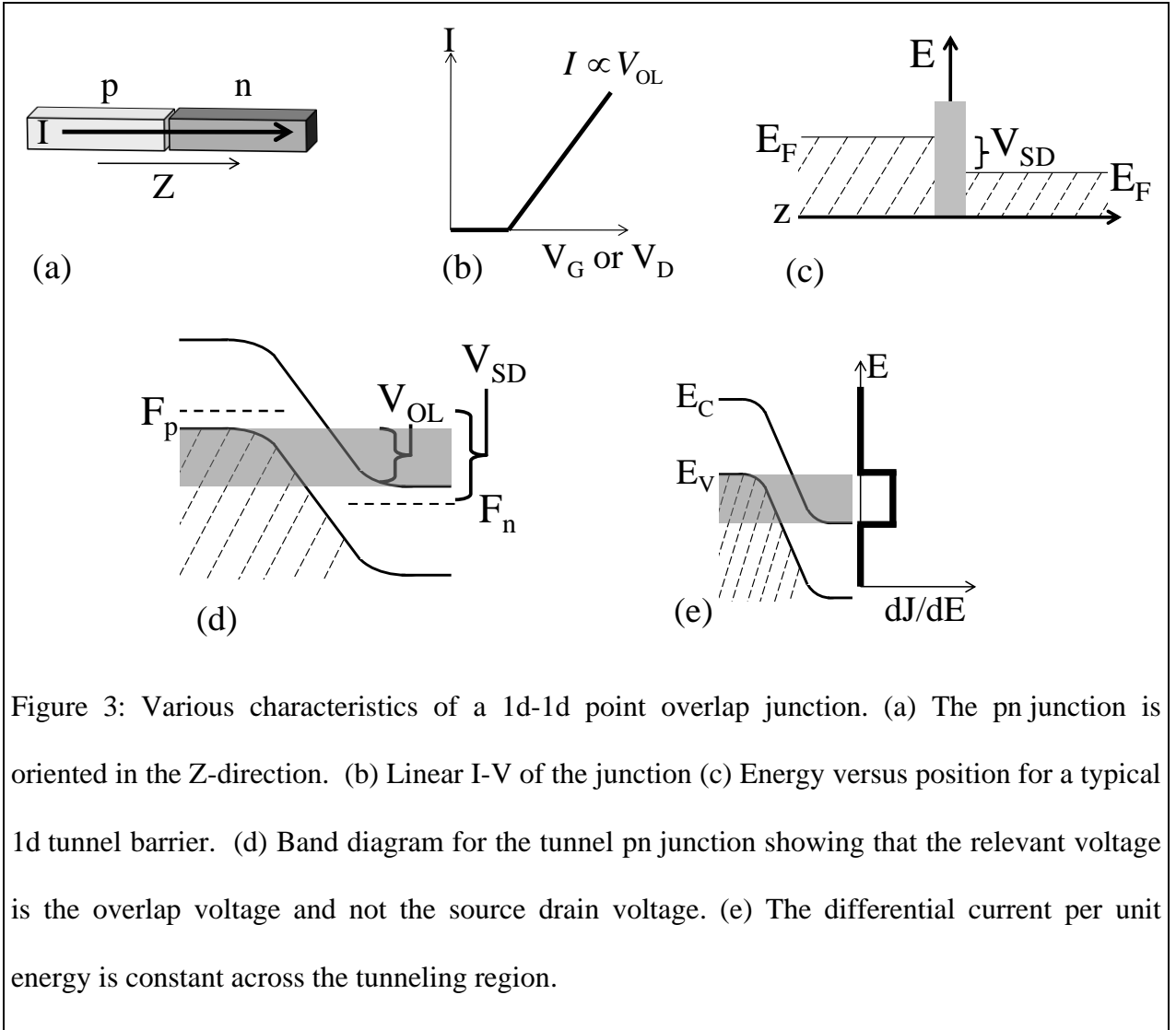
In the following sections we analyze each of the nine cases, in the following sections:

II. 1d-1d; III. 3d-3d; IV. 2d-2d_{edge}; V. 0d-1d; VI. 2d-3d; VII. 1d-2d; VIII. 0d-0d; IX. 2d-2d_{face};

X. 1d-1d_{edge}. We ask which are promising for adaptation into a TFET⁷, or for a new generation^{8,9,10,11} of Backward Diodes?

II. 1d-1d Point Junction

A 1d-1d point pn junction describes tunneling¹² within a nanowire or carbon nanotube junction as schematically represented in Fig. 3(a). Tunneling is occurring from the valence band p-side to the conduction band n-side. The gate is not shown as there are many possible gate



geometries. The band diagram across this junction is given by Fig. 3(d).

In analyzing all of the devices, we consider a direct gap semiconductor with a small gate bias. In particular we consider the regime near the band overlap turn-on where a small change in gate voltage (k_bT/q or less) will result in a large change in the density of states but only a small change in the dimensionless tunneling probability. Consequently we assume that the tunneling probability is roughly a constant, $\mathcal{T}_{\text{device}}$, and will not change significantly for small changes in the gate voltage.

We also define V_{OL} to be the overlap voltage between the conduction and valence bands as shown in Fig. 1(b). In a backward diode structure this would be related to the reverse bias. In a transistor structure, this would typically be related to the gate voltage, V_G , and the source drain bias voltage, V_{SD} . In order to keep the analysis as simple and general as possible we will use the band overlap voltage, V_{OL} in all of the analyses instead of V_G or V_{SD} .

The 1d nanowire current can be derived as an adaptation of the normal quantum of conductance, $2q^2/h$, approach. The band diagram for the typical quantum of conductance is shown in Fig. 3(c). The current flow is controlled by the difference in the Fermi levels, which is the source drain voltage, V_{SD} , as shown. Current is given by charge \times velocity \times density of 1d states. Furthermore, the differential current, dI/dE , that flows at any given energy is the same at all energies. This arises because the energy dependence of the velocity and 1d density of states exactly cancel, such that current is the same regardless of the energy. This results in a current I , controlled by quantum conductance where $(I=2q^2/h) \times V_{\text{SD}} \times \mathcal{T}_{\text{device}}$, where $\mathcal{T}_{\text{device}}$ is the tunneling probability.

Now to properly consider the transition from conduction band to valence band we look at the band diagram given in Fig. 3(d). Initially, we consider the situation shown in Fig. 3(d),

where the valence band on the p-side of the junction is completely full and the conduction band on the n-side is completely empty. This would correspond to non-degenerate doping, $V_{SD} > k_b T/q$ and $V_{SD} > V_{OL}$.

As shown in Fig. 3(d), the band edges cut off the number of states that can contribute to the current. Unlike a single band 1d conductor, the overlap voltage V_{OL} determines the amount of current that can flow. Nevertheless, as shown in Fig. 3(e), dJ/dE is independent of energy and is equal to q/h . This arises because the exact same energy dependence cancellation between the velocity and density of states still occurs on both sides of the 1d pn junction.

Thus the 1d pn junction will conduct with a quantum of conductance times the tunneling probability, with the relevant voltage being the overlap voltage.

$$I_{1d-1d} = \frac{2q^2}{h} \times V_{OL} \times \mathcal{T}_{\text{device}} \quad (2.1)$$

Since a long-range goal is a powering and switching voltage $< k_b T/q$, let us consider the case $V_{SD} < k_b T/q$. In this small bias regime everything of interest occurs within a $k_b T$ or two of energy. Consequently we can Taylor expand the Fermi occupation difference ($f_c - f_v$):

$$f_c = \frac{1}{e^{(E - E_{Fc})/k_b T} + 1} \quad (2.2)$$

$$f_c - f_v \approx \frac{(E_{Fc} - E_{Fv})}{4k_b T} \approx \frac{qV_{SD}}{4k_b T} \quad (2.3)$$

Thus the ultimate effect of the small differential Fermi occupation factors is to multiply the low temperature current by the factor $qV_{SD}/4k_b T$. We can therefore write a conductance for small source drain biases:

$$G_{1d-1d} = \frac{2q^2}{h} \times V_{OL} \times \mathcal{T}_{\text{device}} \times \frac{q}{4k_b T} \quad (2.4)$$

This is true for all of the following devices to be considered in this article, as well. Thus we will continue to make the approximation that the valence band is full and the conduction band is empty when calculating the potential current flow, and then add the effect of the partial Fermi occupation functions afterwards. A more rigorous derivation of the tunneling current and the effect of the Fermi functions are given in Appendix A.

III. 3d-3d Bulk Junction

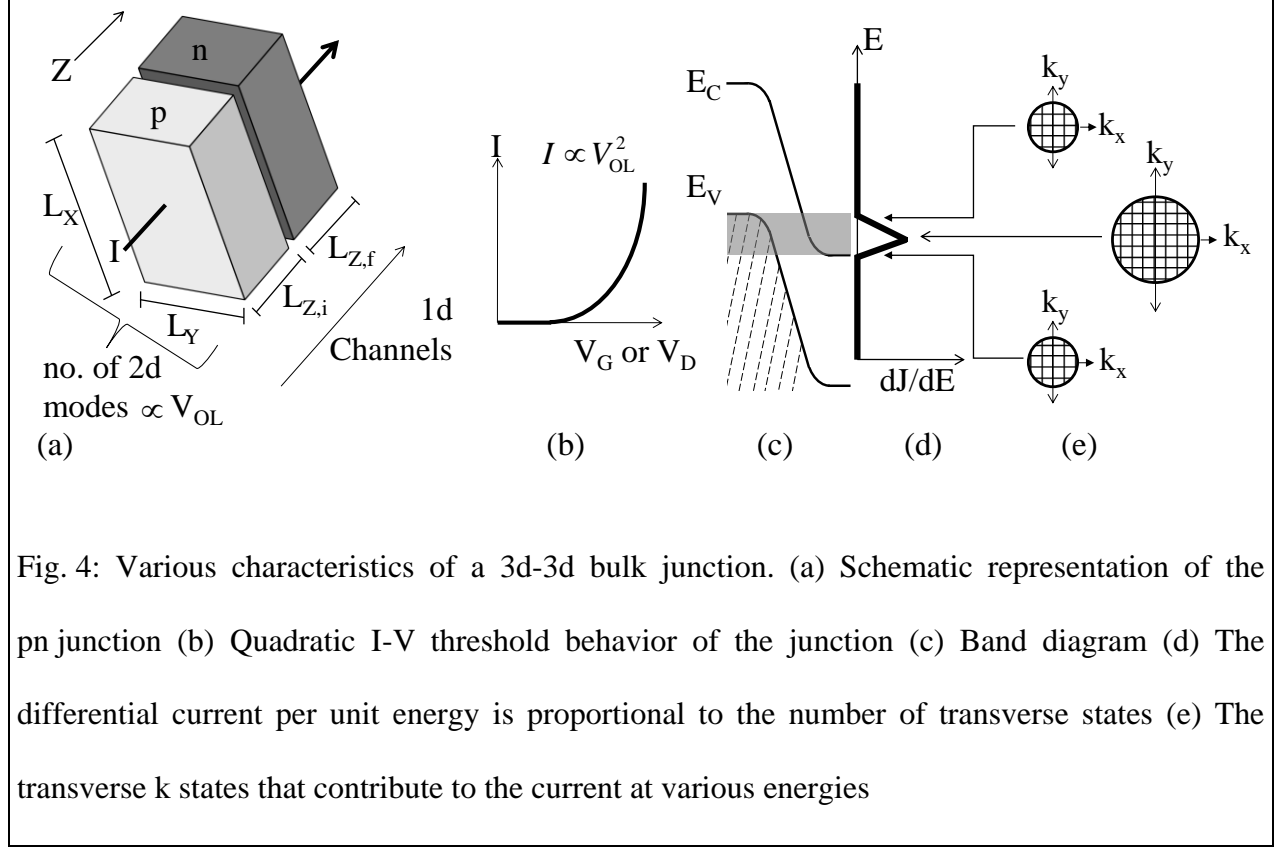
A 3d-3d junction simply means a pn junction or heterojunction where there is a bulk semiconductor on either side of the sample. A generalized schematic of the tunneling junction only is shown in Fig. 4(a). The band diagram across this junction is given by Fig. 4(c).

The 3-d bulk current can be derived from a few simple considerations. The junction is a large 2d surface and can be considered to be a 2d array of 1d channels. The 2d array is defined by the transverse k-states that can tunnel. Each 1d channel is equivalent to the 1d-1d case described in the previous section and will conduct with a quantum of conductance times the tunneling probability. The differential current density can therefore be written as:

$$\partial I = N_{\perp \text{ states}} \times \frac{2q}{h} \times \mathcal{T}_{\text{device}} \times \partial E \quad (3.1)$$

The number of transverse states is the number of k-states within the maximum transverse energy at a given energy. The transverse energy is limited by the closest band edge and peaks in the middle of the overlap. This is shown in Fig. 4(e). The differential current density is given by Fig. 4(d). Integrating over the overlap gives:

$$\begin{aligned} I_{3d-3d} &= \frac{1}{2} \left(\frac{Am^*}{2\pi\hbar^2} \times \frac{qV_{OL}}{2} \right) \times \frac{2q^2}{h} V_{OL} \times \mathcal{T}_{\text{device}} \\ &= \text{No. of 2d Channels} \times \text{1d Conductance} \end{aligned} \quad (3.2)$$



for large $V_{OL} > k_b T/q$ where A is the area of the junction.

For small $V_{OL} < k_b T/q$ the conductance can be written as:

$$G_{3d-3d} = \frac{1}{2} \left(\frac{A m^*}{2\pi \hbar^2} \times \frac{q V_{OL}}{2} \right) \times \frac{2q^2}{h} V_{OL} \times \tau_{device} \times \frac{q}{4k_b T} \quad (3.3)$$

Thus for very small gate biases the current is quadratic in the gate voltage as shown in Fig. 4(b). This is the exact same result that comes from taking the appropriate limits of Kane's tunneling theory¹³.

In the Appendix, we also formally derive this result in a different manner using the transfer Hamiltonian method^{14,15,16,17}. We do this as an alternative, employing the more modern channel conductance approach. The transfer Hamiltonian method was first used by Oppenheimer to study the field emission of hydrogen¹⁷. It was then expanded by Bardeen¹⁴ for tunneling in superconductors and then the case of independent electrons was considered by

Harrison¹⁶. The transfer Hamiltonian method in the Appendix is just an application of Fermi's golden rule with a clever choice of states and perturbing Hamiltonian.

IV. 2d-2d Edge Junction

A 2d edge overlapped junction describes a junction where the tunneling occurs along a line separating p and n regions within in a 2d confined surface. The junction is schematically represented in Fig. 5(a). This could be represented by a case where tunneling occurs within a thin inversion region near a surface or within an ultra-thin body device.

The derivation of the current is almost identical to the 3d-3d case, except that instead of having a 2d array of 1d channels we now have a 1d array of 1d channels. Therefore the current is:

$$I_{2d-2d,edge} = \frac{2}{3} \left(\frac{L_X \sqrt{m^*}}{\pi \hbar} \times \sqrt{q V_{OL}} \right) \times \left(\frac{2q^2}{h} \times V_{OL} \times \mathcal{T}_{device} \right) \quad (4.1)$$

= No. of 1d Channels \times 1d Conductance

for large $V_O > k_b T/q$ where L_X is the length of the junction.

For small $V_{OL} < k_b T/q$ the conductance can be written as:

$$G_{2d-2d,edge} = \frac{2}{3} \left(\frac{L_X \sqrt{m^*}}{\pi \hbar} \times \sqrt{q V_{OL}} \right) \times \left(\frac{2q^2}{h} \times V_{OL} \times \mathcal{T}_{device} \right) \times \left(\frac{q}{4k_b T} \right) \quad (4.2)$$

Thus for very small gate biases the current is proportional to $V_{OL}^{3/2}$ as shown in Fig. 5(b). Similar to the 3d case, the number of transverse states that can tunnel varies with energy and needs to be properly integrated. As shown in Fig. 5(d) and 5(e), the differential current density is proportional to the number of states that can tunnel. The number of 1d states is proportional to the square root of the energy and so the differential current density follows a square root with respect to energy.

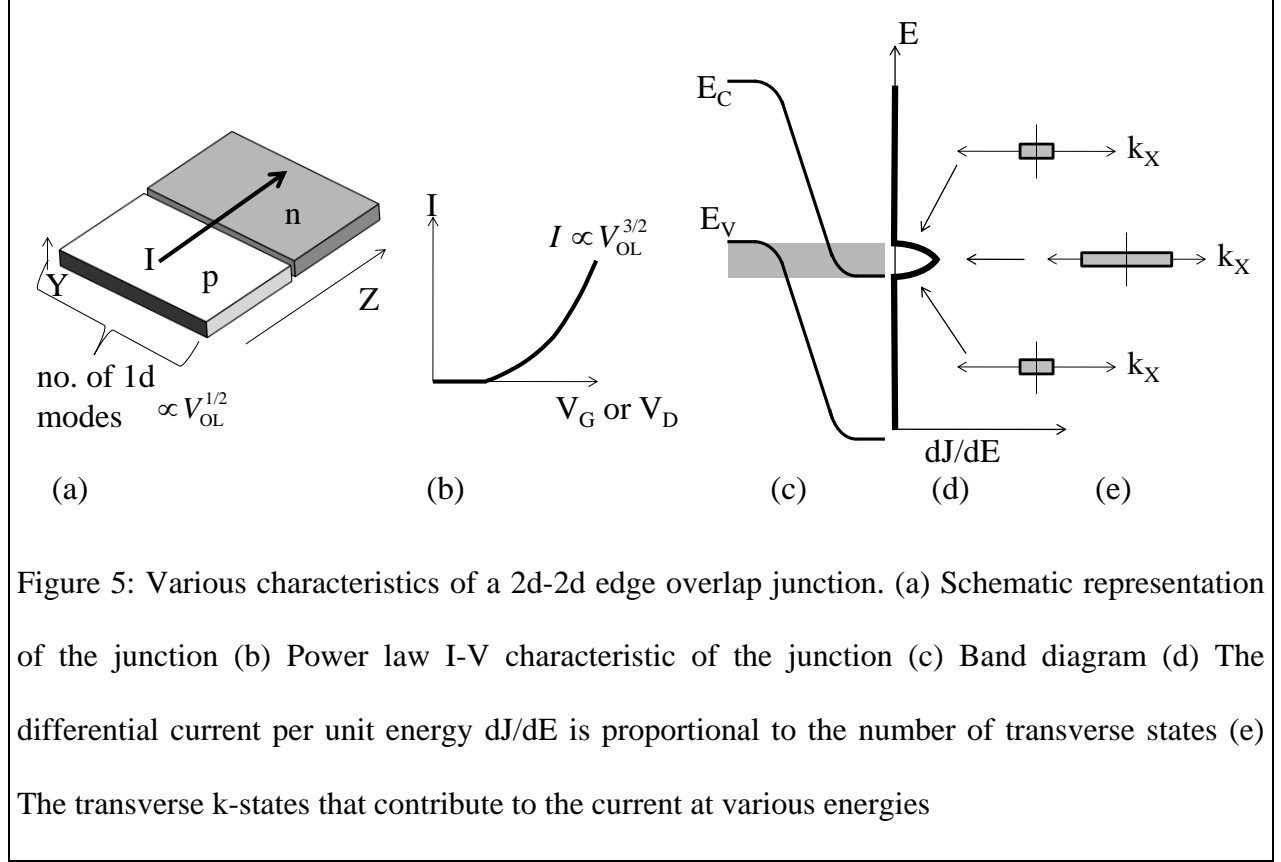
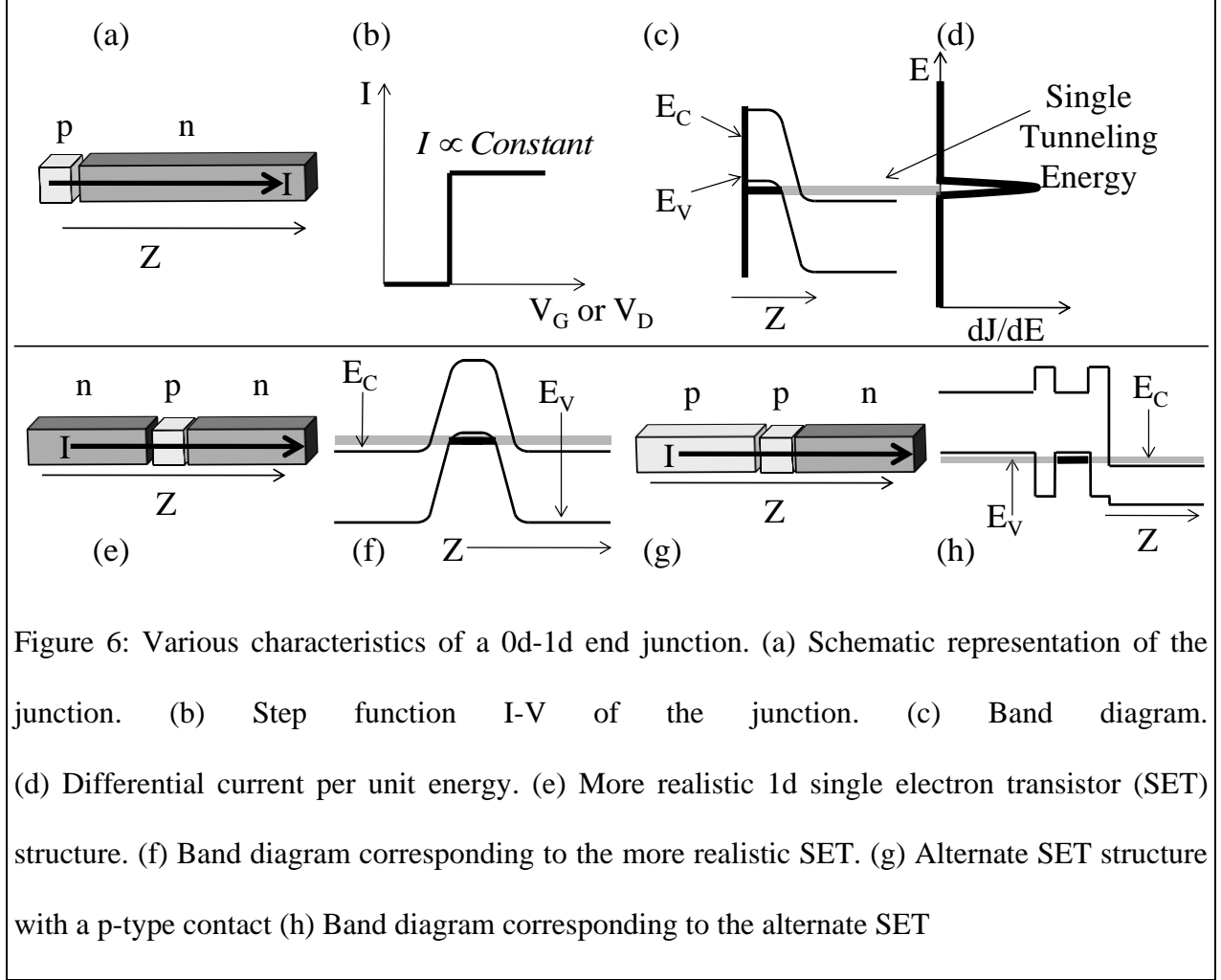


Figure 5: Various characteristics of a 2d-2d edge overlap junction. (a) Schematic representation of the junction (b) Power law I-V characteristic of the junction (c) Band diagram (d) The differential current per unit energy dJ/dE is proportional to the number of transverse states (e) The transverse k -states that contribute to the current at various energies

V. 0d-1d Junction

A 0d to 1d junction represents tunneling from a quantum dot to a nanowire as shown in Fig. 6(a). Our main goal in analyzing this case is to provide the basis for analyzing higher dimensionality systems such as a 2d-3d or 1d-2d junctions. Consequently we consider two different 0d-1d systems. First we will assume that there is an electron in the quantum dot and find the rate at which it escapes into the end of a 1d wire. In reality, there is no way to electrically contact the quantum dot. Therefore we consider a more realistic situation that includes the need to couple current into the dot. This case essentially evolves into a single electron transistor (SET) as shown in Fig. 6(e) and 6(g).



The rate at which an electron escapes from the quantum dot into a nanowire is given by the field ionization of a single state such as an atom. In Gamow's model of alpha particle decay¹⁸, the particle is oscillating back and forth in its well and it attempts to tunnel on each round trip oscillation. If the dot has a length of L_Z along the tunneling direction, the electron will travel a distance of $2L_Z$ between tunneling attempts. Its momentum is given by $p_Z = mv_Z = \hbar k_Z$ where $k_Z = \pi/L_Z$ in the ground state. Using $E_Z = \hbar^2 k_Z^2 / 2m$, the time between tunneling attempts is $\tau = 2L_Z / v_Z = \hbar / 2E_Z$. The tunneling rate per second is $R = (1/\tau) \times T_{\text{device}}$. This can be converted to a current by multiplying by the electron charge, and a factor 2 for spin to give:

$$I = \frac{4q}{h} \times E_Z \times \mathcal{T}_{\text{device}} \quad (5.1)$$

This is the same result that one obtains from the transfer Hamiltonian method outlined in the Appendix. It also assumes a large source drain bias, as usual. These simple considerations predict a constant current as soon as the bands overlap as shown in Fig. 6(b). As seen from the band diagram in Fig. 6(c), all tunneling occurs at the single confined energy.

To include coupling into the dot, we add a second nanowire to supply current, as shown in Fig. 6(e) or 6(g). We assume that the second nanowire has the same tunneling probability/coupling strength to the quantum dot as the original one. The new band diagram is shown in Fig. 6(f) or 6(h), and resembles that of a “single electron transistor”¹⁹. As in Fig. 6(c), the tunneling occurs at a single energy and will result in a constant current once the bands overlap. The tunneling event into the dot follows sequentially after tunneling out. Therefore the total current tunneling transport rate is halved $(1/2\tau) \times \mathcal{T}_{\text{device}}$, and the current is cut in half:

$$I = \frac{2q}{h} \times E_Z \times \mathcal{T}_{\text{device}} \quad (5.2)$$

$I = (2q/h)E_Z \mathcal{T}_{\text{device}}$ applies to a filled dot, and an empty 1d wire. If there is partial Fermi-Dirac occupation on both sides we can define a conductance based on the Fermi Level difference:

$$G = \frac{2q}{h} \times E_Z \times \mathcal{T}_{\text{device}} \times \frac{q}{4k_b T} \quad (5.3)$$

While our simple model assumes a perfectly sharp level and therefore a step turn-on in the current, in reality the level will be broadened and the turn-on threshold will assume the shape of the level broadening. This broadening can be extrinsically caused by any inhomogeneities in the lattice such as defects, dopants, or phonons. Even without these effects, simply coupling to the dot to the nanowires will already cause a significant amount of broadening²⁰. In the simplest

model, the density of states in the level broadens to form a Lorentzian with a full width in energy at half maximum of γ . We seek to find γ , since that will determine the inherent broadening at threshold. We start with the escape rate of electrons from the dot $= (4E_Z/h) \times T_{\text{device}}$, where the escape rate is doubled, since there are two extra wires that can capture the escaped electron. Multiplying by \hbar leads to a broadening:

$$\gamma = (2/\pi) \times E_Z \times T_{\text{device}} \quad (5.4)$$

which allows us to write the conductance as $G = (q^2/h) \times \gamma \times (\pi/4k_b T)$.

We can now define a Figure-of-Merit for 0d-1d switches:

$$\frac{\text{Conductance}}{\text{Broadening}} = \frac{G}{\gamma} = \frac{\pi q^2/h}{4k_b T} \quad (5.5)$$

which can be rewritten as:

$$\frac{G}{q^2/h} = \frac{\pi \gamma}{4k_b T} \quad (5.6)$$

This means that a steep switch with broadening $\gamma \ll k_b T$, must come at the expense of a conductance much less than the conductance quantum $G \ll (q^2/h)$.

VI. 2d-3d Junction

A 2d-3d tunneling junction is typical in vertical² TFET's where the tunneling occurs from the bulk to a thin confined layer under the gate. The thin layer can either be a thin inversion layer or a physically separate material. A generalized schematic of this tunnel junction is shown in Fig. 7(a). Here the z-axis is rotated 90° from what one would usually expect so that the axes remain parallel between figures.

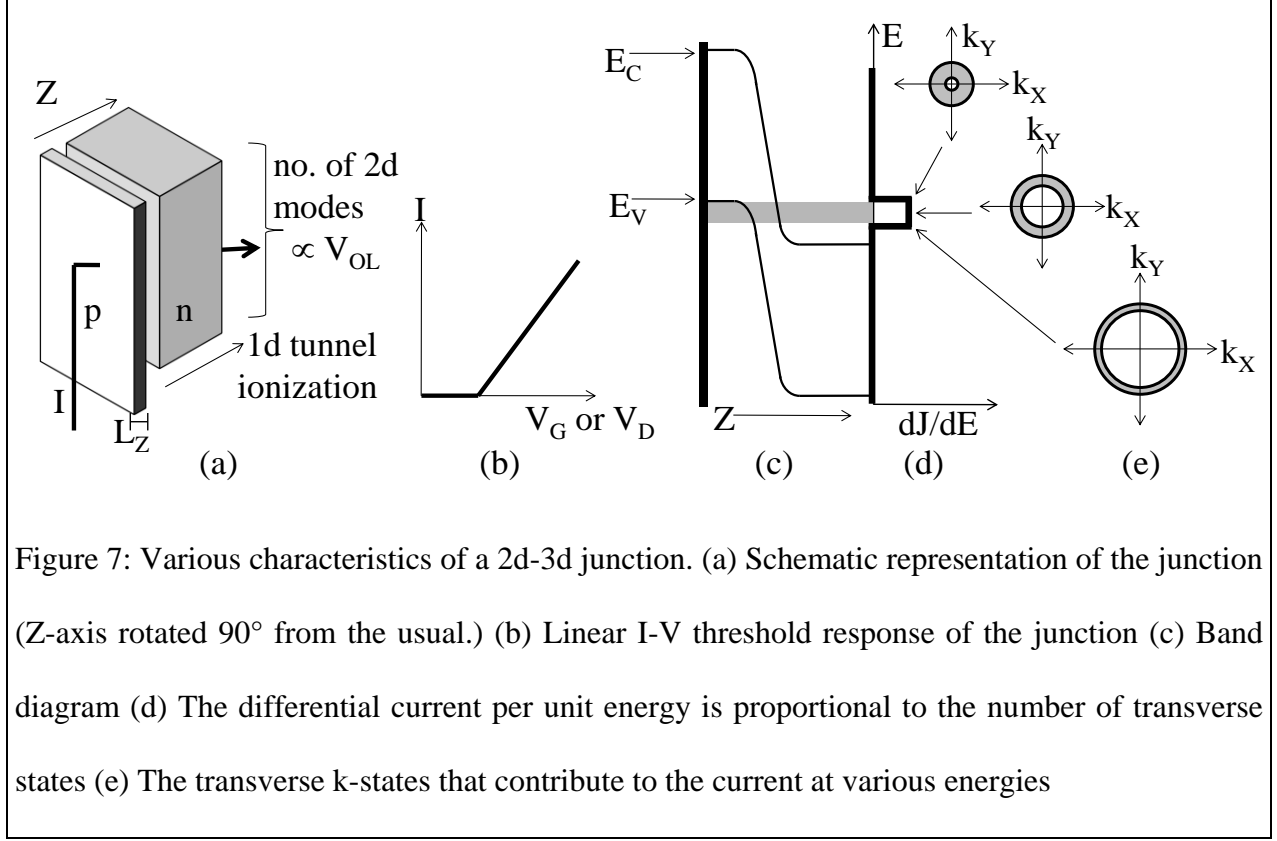


Figure 7: Various characteristics of a 2d-3d junction. (a) Schematic representation of the junction (Z-axis rotated 90° from the usual.) (b) Linear I-V threshold response of the junction (c) Band diagram (d) The differential current per unit energy is proportional to the number of transverse states (e) The transverse k-states that contribute to the current at various energies

The derivation for this case is very similar to the 3d-3d case. As in that section, the junction is a large 2d surface and can be considered to be a 2d array of 1d tunneling problems. However, this case does not represent the typical 1d quantum of conductance. In this case, the 1d problem is better described by the field ionization of a single state such as an atom as described in the 0d-1d section. We simply multiply that result by the number of 2d channels to get a current of:

$$I = \text{No. of 2d channels} \times \text{1d field ionization}$$

$$I = \left(\frac{Am}{2\pi\hbar^2} \times \frac{qV_{OL}}{2} \right) \times \left(\frac{4q}{h} \times E_Z \times \tau_{\text{device}} \right) \quad (6.1)$$

for large $V_{OL} > k_b T/q$.

For small $V_{OL} < k_b T/q$ the conductance can be written as:

$$G_{2d-3d} = \left(\frac{Am}{2\pi\hbar^2} \times \frac{qV_{OL}}{2} \right) \times \left(\frac{4q}{h} \times E_Z \times \mathcal{T}_{\text{device}} \right) \times \left(\frac{q}{4k_b T} \right) \quad (6.2)$$

Here, E_Z is the confinement energy of the 2d layer. This is the exact same result that comes from the transfer Hamiltonian method in the Appendix so long as we also assume that the confined electron is in the ground state such that $k_Z = \pi/L_Z$. Thus for very small V_{SD} , or small gate biases, the current is linear in V_{OL} as shown in Fig. 7(b). Compared to the bulk 3d-3d case, confining one side of the junction resulted in the replacement of qV_{OL} with $4E_Z$.

To justify the number of transverse states that we have included we need to look more closely at the tunneling process. The band diagram is shown in Fig. 7(c). Since the tunnel rate from the 2d quantum well states is constant, the differential current per unit energy is exactly proportional to the number of states that tunnel at any given energy. The number of states that tunnel is equal to the number of transverse states, and since the 2d density of states is independent of energy, the differential current per unit energy is also a constant. Fig. 7(e) shows that the states that tunnel at any given energy map out a ring in k-space of constant area. Oddly, the figures also show current flowing in only the upper half of the energy overlap region, at low kinetic energy in the valence band. At higher kinetic energy in the valence band, the transverse momentum becomes too large to fit into the small region of k-space on the conduction band side. Thus only valence band states with a kinetic energy up to $V_{OL}/2$ will tunnel.

Current can flow in along the transverse direction as shown in Fig. 7(a). Other methods can also be considered for making electrical contact.

VII. 1d-2d Junction

A 1d-2d junction describes tunneling between the edge of a nanowire and a 2d sheet as shown in Fig. 8(a). The derivation for this case is very similar to the 2d-3d case. The only difference is that instead of a 2d array of 1d tunneling, we now have a 1d array of 1d tunneling. Thus the current is:

$$I_{1d-2d} = \text{no. of 1d channels} \times \text{1d tunnel ionization}$$

$$I_{1d-2d} = \left(\frac{L_x}{\pi \hbar} \times \sqrt{q m^* V_{OL}} \right) \times \left(\frac{4q}{h} \times E_Z \times \mathcal{T}_{\text{device}} \right) \quad (7.1)$$

for large $V_{OL} > k_b T/q$.

For small $V_{OL} < k_b T/q$ the conductance can be written as:

$$G_{1d-2d} = \left(\frac{L_x}{\pi \hbar} \times \sqrt{q m^* V_{OL}} \right) \times \left(\frac{4q}{h} \times E_Z \times \mathcal{T}_{\text{device}} \right) \times \left(\frac{q}{4k_b T} \right) \quad (7.2)$$

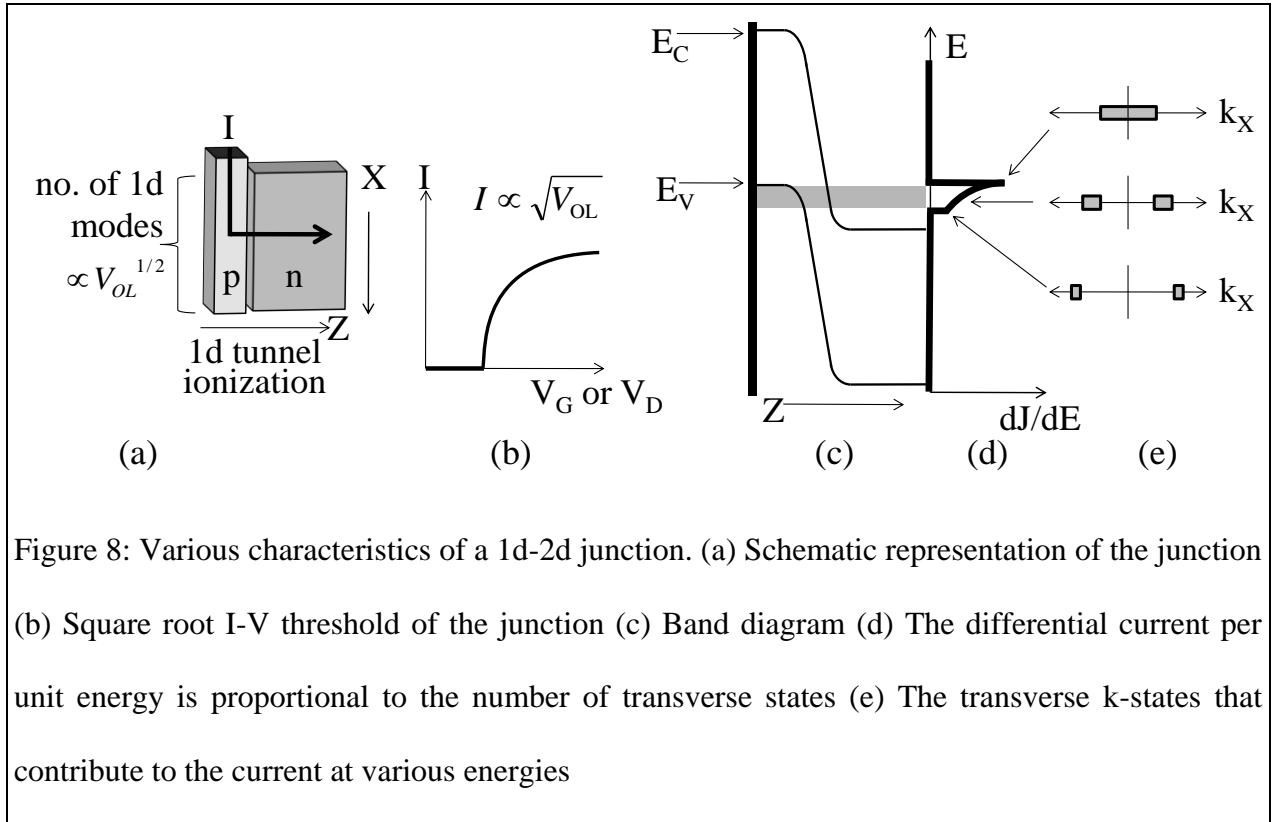


Figure 8: Various characteristics of a 1d-2d junction. (a) Schematic representation of the junction (b) Square root I-V threshold of the junction (c) Band diagram (d) The differential current per unit energy is proportional to the number of transverse states (e) The transverse k -states that contribute to the current at various energies

where, E_Z is the confinement energy along z -axis of the 1d layer. This is exactly the same result that comes from the transfer Hamiltonian method in the Appendix as long as we also assume that the confined electron is in the ground state such that $k_Z = \pi/L_Z$ as before. Thus for very small V_{OL} the current is proportional to $\sqrt{V_{OL}}$ as shown in Fig. 8(b). In addition, comparing to the 2d-2d edge overlap formula, confining one side of the junction resulted in the replacement of qV_{OL} with $3E_Z$.

As in the 2d-3d case, current flows in only the upper half of the energy overlap region at low kinetic energy in the valence band, due to conservation of transverse momentum. This is indicated by the shaded part of the band diagram in Fig. 8(c). At higher kinetic energy in the valence band, the transverse momentum becomes too large to fit into the small region of k -space on the conduction band side. Therefore, we included transverse states only up to half the overlap voltage. In this case, the 1d density of states varies with energy and so the current that tunnels at different energies is different. This is shown in Fig. 8(d). Fig. 8(e) shows which transverse states contribute at each energy.

VIII. 0d-0d Quantum Dot Tunneling

This case simply represents tunneling from a filled valence band quantum dot to an empty conduction band quantum dot. It is schematically represented in Fig. 9(a). In order to create a meaningful device the quantum dots need to be coupled to contacts, to pass current in and out of the device. This coupling is indicated by the tunnel junctions in Fig. 9(a). By itself this case is not very interesting, but it will be useful for describing some of the other cases. As with the 0d-1d case, we will consider two different 0d-0d systems. Initially we will ignore the effects of the contacts to the dots and then we will include the effects of contacting the quantum dots in order to make a realistic device.

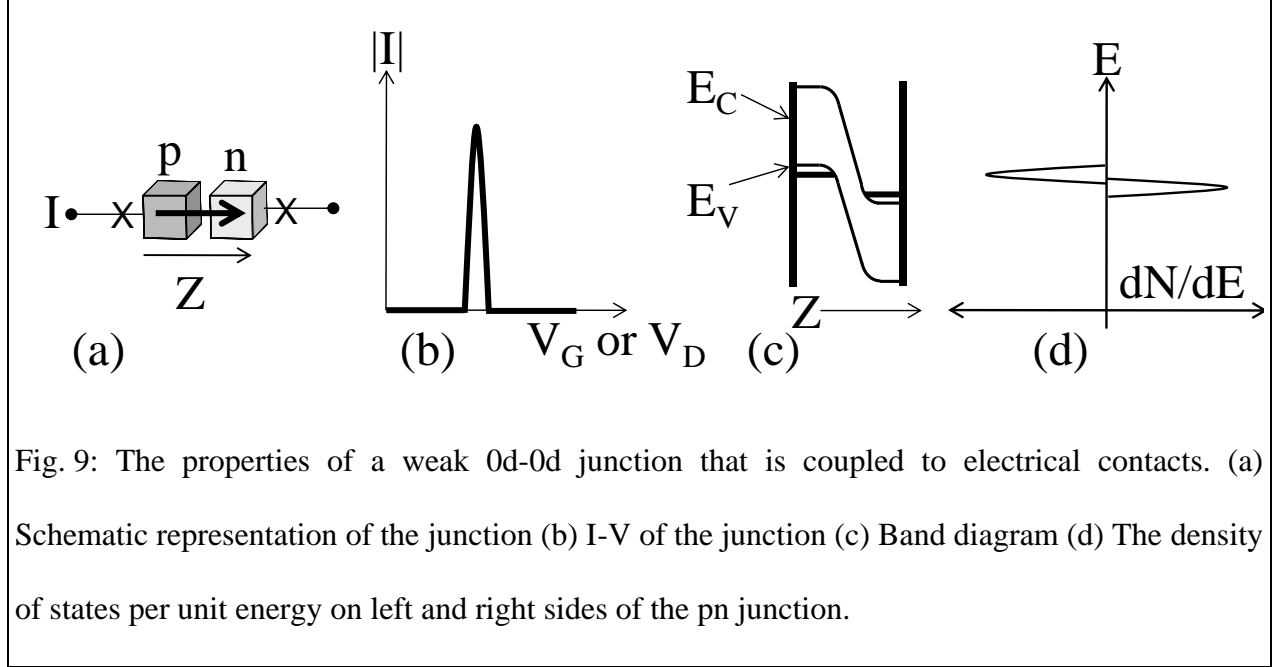


Fig. 9: The properties of a weak 0d-0d junction that is coupled to electrical contacts. (a) Schematic representation of the junction (b) I-V of the junction (c) Band diagram (d) The density of states per unit energy on left and right sides of the pn junction.

If we have two isolated quantum dots that are coupled to each other with an electron in one of the dots, the electron will quantum mechanically oscillate back and forth between the dots. The band diagram for this situation is shown in Fig. 9(c). The thick lines represent the confined energy levels. In order to calculate the rate at which the electron travels between the two states we need to use time dependent perturbation theory (TDPT). The standard result from TDPT for the transition probability of a two level system subject to a constant perturbation is²¹:

$$P_{i \rightarrow f}(t) = 4 \frac{|M_{fi}|^2}{\hbar^2} \frac{\sin^2(\omega_{fi} t/2)}{\omega_{fi}^2} \quad (8.1)$$

Where $\omega_{fi} = (E_f - E_i)/\hbar$ and M_{fi} is the transition matrix element between the states as defined in Appendix A. In the Appendix we derived the current using Fermi's golden rule. Evaluating the matrix element is similar and is given by Eq'n. (A.12):

$$|M_{fi}|^2 = \frac{1}{\pi^2} E_{Z,i} \times E_{Z,f} \times \mathcal{T}_{\text{device}} \quad (8.2)$$

Plugging Eq'n. (8.2) into Eq'n. (8.1) gives:

$$P_{i \rightarrow f}(t) = \frac{4}{\hbar^2 \pi^2} E_{Z,i} \times E_{Z,f} \times T_{\text{device}} \times \frac{\sin^2(\omega_{fi} t/2)}{\omega_{fi}^2} \quad (8.3)$$

Here, $E_{Z,i}$ is the confinement energy along the z-axis of the initial dot and $E_{Z,f}$ is the confinement energy along the z-axis of the final dot. Thus the probability that the electron is in the final dot oscillates back and forth and its magnitude is set by the confinement energies in each dot, as given in Eq'n. (8.3).

Now we consider what happens when the electrical contacts couple to the dot. The levels in the quantum dots will broaden due to the contact coupling and will have a broadened density of states as shown in Fig. 9(d). When the quantum dots are aligned, current will flow. This results in a single peak in the I-V curve as shown in Fig. 9(b). The width of the current peak is determined by the contact broadening. For a single level coupled to a single contact the energy broadening will be $\gamma = \hbar/\tau = \hbar I/q$. As in Section V, the electron's escape rate is analogous to the attempt frequency of Gamow's theory¹⁸ of alpha decay tunneling and is given by $2E_{Z,i}/\hbar$. The maximum current to the contact per spin state is half of Eq'n. (5.1): $I = (2q/\hbar) \times E_{Z,i} \times T_{\text{contact}}$, where the contact tunneling transmission is labeled T_{contact} to distinguish it from the interdot transmission T_{device} . Consequently, the broadening will be given by:

$$\gamma = (1/\pi) \times E_Z \times T_{\text{contact}} \quad (8.4)$$

For simplicity, we assume that the confinement energies are the same in both dots:

$$E_{Z,i} = E_{Z,f} = E_Z.$$

The transition probability, Eq'n. (8.3), resembles a delta function, which when integrated leads to Fermi's Golden Rule: $\text{Rate} = \frac{2\pi}{\hbar} |M_{fi}|^2 \frac{dN}{dE}$, where dN/dE is the density of final states.

In the 0d case, there is only one state, and so the density of states is the inverse of the broadening, γ : $dN/dE=1/\gamma = \pi/(E_Z \times \mathcal{T}_{\text{contact}})$. The transition rate leads to a current:

$$I = 2q \frac{2\pi}{\hbar} |M_{fi}|^2 \frac{\pi}{E_Z \times \mathcal{T}_{\text{contact}}} \quad (8.5)$$

$$I = 2q \frac{2\pi}{\hbar} \left[\frac{1}{\pi^2} E_Z \times E_Z \times \mathcal{T}_{\text{device}} \right] \frac{\pi}{E_Z \times \mathcal{T}_{\text{contact}}} \quad (8.6)$$

$$I = \frac{4q}{\hbar} E_Z \times \frac{\mathcal{T}_{\text{device}}}{\mathcal{T}_{\text{contact}}} \quad (8.7)$$

We will show in Section XI that the condition for perturbation theory to be valid requires that the interdot tunneling transmission $\mathcal{T}_{\text{device}}$ be less than the square contact tunneling transmission: $\mathcal{T}_{\text{device}} \ll (\mathcal{T}_{\text{contact}})^2$. This assures that the interdot current is always less than the maximum contact current. Eq'n. (8.7) can now be adapted to allow for Fermi occupation of the dots, which leads to a conductance:

$$\sigma = \frac{4q}{\hbar} E_Z \times \frac{\mathcal{T}_{\text{device}}}{\mathcal{T}_{\text{contact}}} \times \frac{q}{4k_b T} \quad (8.8)$$

We can now define a Figure-of-Merit for 0d-0d switches as before:

$$\frac{\text{Conductance}}{\text{Broadening}} = \frac{G}{\gamma} = \frac{8\pi^2 q^2 / h}{4k_b T} \times \frac{\mathcal{T}_{\text{device}}}{\mathcal{T}_{\text{contact}}^2} \quad (8.9)$$

which can be rewritten as:

$$\frac{G}{q^2/h} = \frac{2\pi^2 \gamma}{k_b T} \times \frac{\mathcal{T}_{\text{device}}}{\mathcal{T}_{\text{contact}}^2} \quad (8.10)$$

Since the perturbation condition, Eq'n. (11.4), is that $[\mathcal{T}_{\text{device}}/(\mathcal{T}_{\text{contact}})^2] < 1$, this places an upper limit on the conductance $G/(q^2/h) < 2\pi^2 \gamma / (k_b T)$. This means that a steep switch with broadening

$\gamma \ll k_b T$, must come at the expense of a conductance much less than the conductance quantum $G \ll (q^2/h)$.

IX. 2d-2d Face Overlap

A 2d-2d area overlapped junction describes tunneling from one quantum well to another through the face of the quantum well. This is different from resonant interband tunnel diodes²², since the tunneling proceeds from the valence to conduction bands. The junction is schematically represented in Fig. 10(a). Here the schematic is rotated 90° from what one would usually expect so that the z-axis lines up between figures. This is one of the most interesting cases as it is the closest to a step function turn-on as illustrated in 10(b). The band diagram is shown in Fig. 10(c).

The step function turn on can be seen by considering the conservation of transverse momentum and total energy. This is depicted in Fig. 10(e). The lower paraboloid represents all of the available states in k-space on the left side of the junction and the upper paraboloid represents the available k-space states on the right side of the junction. In order for current to flow the initial and final energy, and wave-vector k , must be the same and so the paraboloids must overlap. However, as seen in the right part of the figure, they can only overlap at a single energy. Furthermore, the joint density of state pairs between valence and conduction band is a constant in energy. Thus the number of state pairs that tunnel is a constant regardless of the overlap energy as seen in Fig. 10(d).

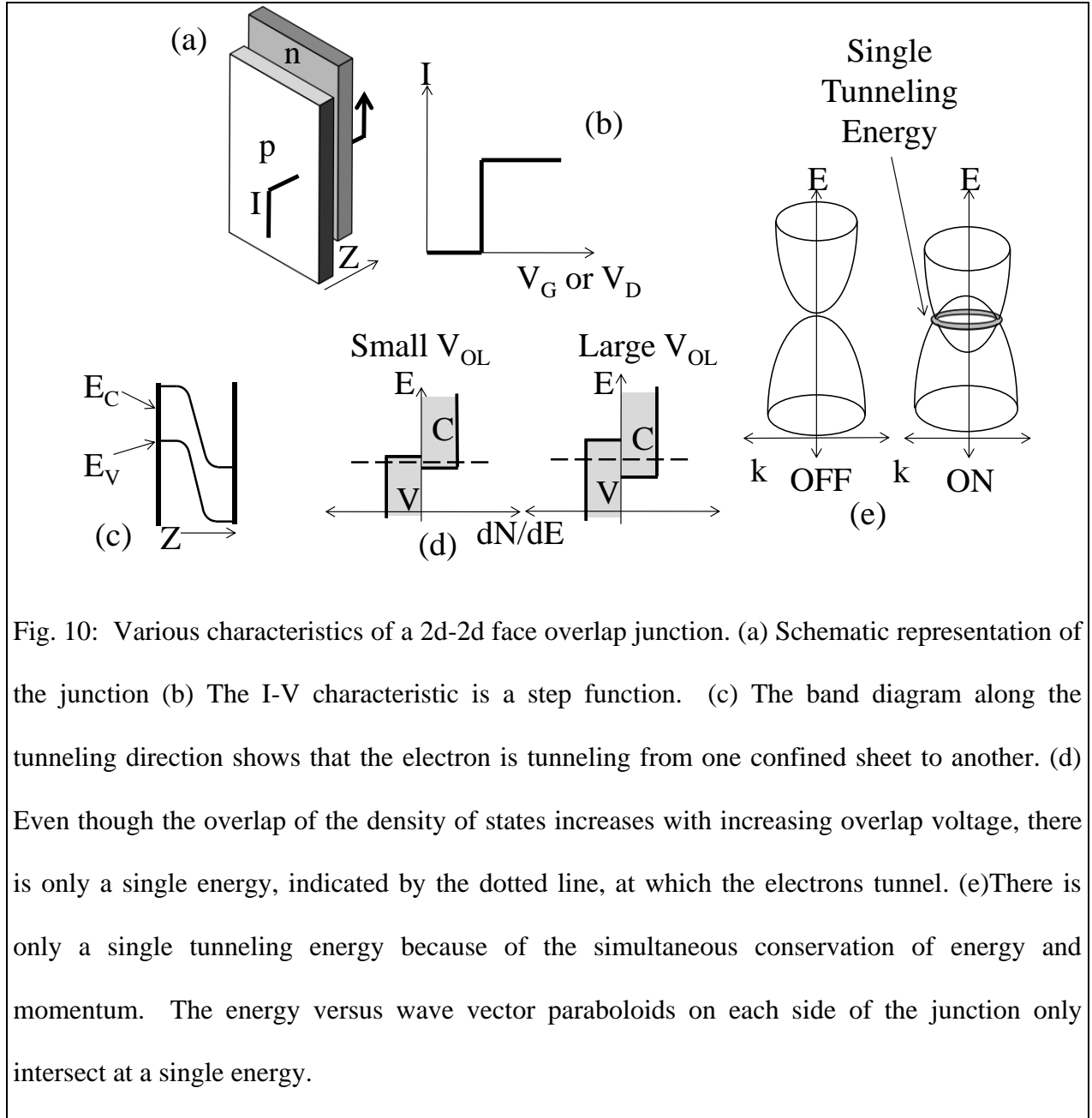


Fig. 10: Various characteristics of a 2d-2d face overlap junction. (a) Schematic representation of the junction (b) The I-V characteristic is a step function. (c) The band diagram along the tunneling direction shows that the electron is tunneling from one confined sheet to another. (d) Even though the overlap of the density of states increases with increasing overlap voltage, there is only a single energy, indicated by the dotted line, at which the electrons tunnel. (e) There is only a single tunneling energy because of the simultaneous conservation of energy and momentum. The energy versus wave vector paraboloids on each side of the junction only intersect at a single energy.

The tunneling rate of the valence/conduction band state pairs that transition is different from the 3d-3d bulk case where we had a 2d array of 1d channels. In this case we have a fixed number of 2d states and a completely different 1d problem. The 1d problem now represents tunneling from a single fixed level to another single fixed level as in the 0d-0d case. As seen from the transition probability in the 0d-0d case, Eq'n. (8.3), the transition probability resembles

a delta function as in Fermi's Golden Rule. This will be integrated below, and is independent of the overlap voltage. Thus the total tunneling current is independent of the overlap voltage and will be a step function with respect to the gate voltage.

In order to calculate the amount of current that flows we need to find the transition rate for each state that tunnels and sum over all of the states that tunnel. Every initial state is coupled to only one final state. This is due to conservation of momentum. This means that we can use the 0d-0d result, Eq'n. (8.3), to describe the transition probability between an initial and final state. Current can flow into each quantum state, along the quantum well, or through the face of the quantum well. We also do not need to externally impose conservation of energy as the 0d-0d result in time dependent perturbation theory is sharply peaked about $E_i=E_f$. Therefore we simply need to sum Eq'n. (8.3) over all initial states or final states:

$$\begin{aligned}\sum P_{i \rightarrow f} &= \frac{Am}{2\pi\hbar^2} \int_0^\infty P_{i \rightarrow f} dE \\ &= \frac{Am}{2\pi\hbar^2} \times \frac{2}{h} E_{Z,i} E_{Z,f} \mathcal{T}_{\text{device}} \times t\end{aligned}\tag{9.1}$$

When evaluating the integral we used equal valence and conduction band mass. Here we see that oscillation in transition probability of individual states is averaged out in summation and that the probability of being in the final state is proportional to time t , as is usual in time-dependent perturbation theory. We also assumed that the bands were sufficiently overlapped and that the lower limit of the integral can be taken to be $-\infty$. This form of Fermi's golden rule is done in Appendix A.

We can then convert this to a transition rate by taking the time derivative. The transition rate can then be converted to a current density by multiplying by the electron charge and 2 for spin to give a current of:

$$I_{2d-2d,face} = \frac{qmA}{\pi^2 \hbar^3} \times E_{Z,i} \times E_{Z,f} \times T_{device} \quad (9.2)$$

for large $V_{SD} > k_B T/q$. For small V_{SD} the conductance depends on the difference in Fermi occupation fractions, and can be written as:

$$G_{2d-2d,face} = \frac{qmA}{\pi^2 \hbar^3} \times E_{Z,i} \times E_{Z,f} \times T_{device} \times \frac{q}{4k_b T} \quad (9.3)$$

The main change in going from 3d-3d to 3d-2d is that the energy factor qV_{OL} became E_Z . Likewise, in going from the 3d-2d to 2d-2d the other energy factor qV_{OL} also became E_Z . Thus for each confined side of the junction the relevant energy changes from the overlap energy to the confinement energy. Consequently the 2d case has roughly the same current as a 3d case if the confinement energy E_Z is the same as the overlap voltage qV_{OL} . In practice E_Z is likely to be much larger than qV_{OL} , providing the 2d-2d case with a significant current boost.

Following the joint density of states, the current takes the form of a step function with respect to the gate voltage. This is similar to the step function case of quantum well optical transitions. As soon as the bands overlap, the current immediately turns on. However, contact broadening mechanisms will smear out the step-like turn-on function and this will be discussed later.

X. 1d-1d Edge Overlap

A 1d-1d edge overlap junction represents two nanowires overlapping each other as shown in Fig. 11(a). This junction is similar to the 2d-2d area overlap. The current can be found by summing the 0d-0d result over a 1d density of states. Alternatively, the method in the appendices will also give the same result. The resulting current is:

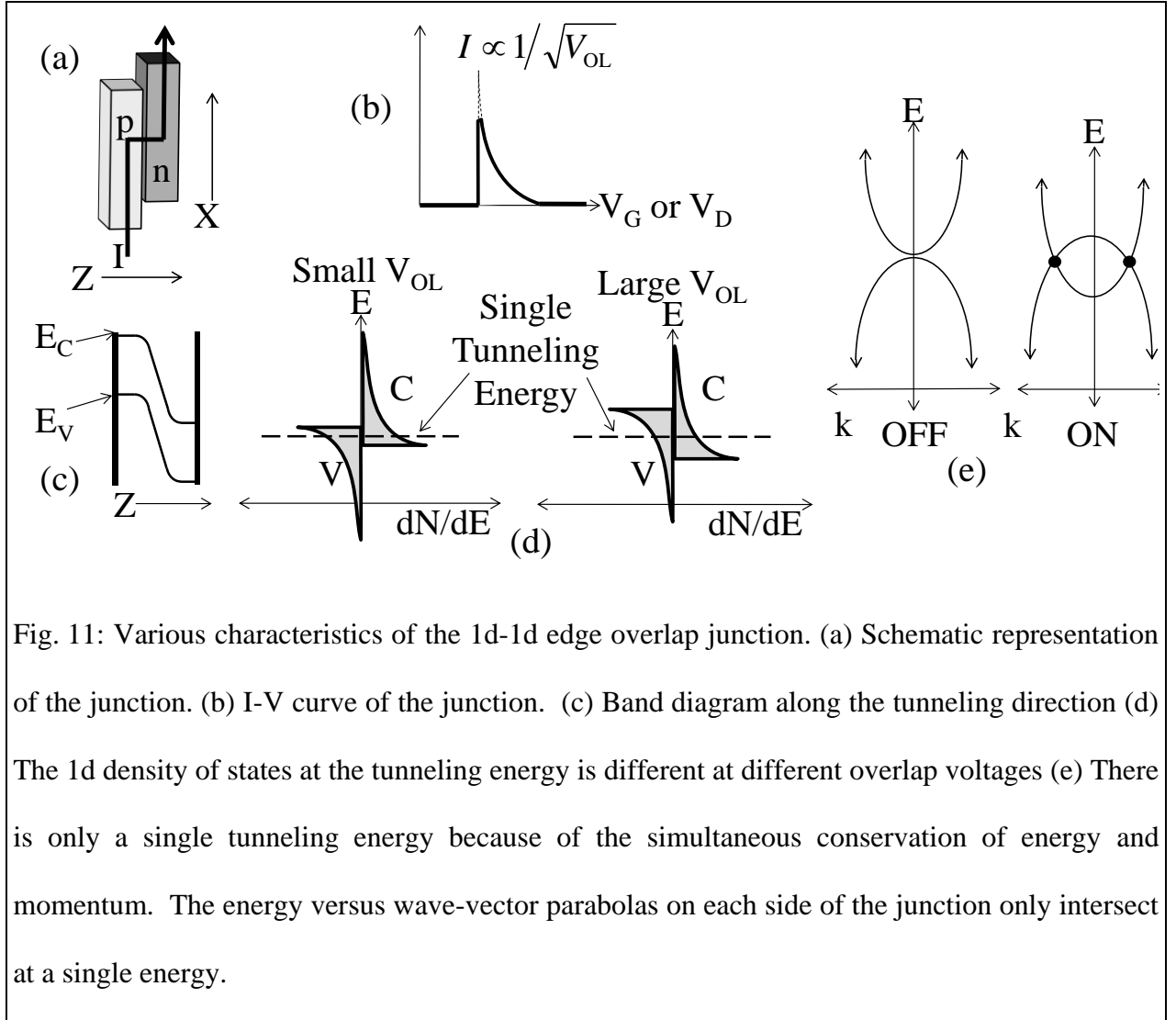
$$I_{1d-1d,edge} = 2 \frac{qL_x}{\pi^2 \hbar^2} E_{Z,i} \times E_{Z,f} \times \sqrt{\frac{m}{qV_{OL}}} \times \mathcal{T}_{device} \quad (10.1)$$

for large $V_{OL} > k_b T/q$.

For small $V_{OL} < k_b T/q$ the conductance can be written as:

$$G_{1d-1d,edge} = 2 \frac{qL_x}{\pi^2 \hbar^2} E_{Z,i} \times E_{Z,f} \times \sqrt{\frac{m}{qV_{OL}}} \times \mathcal{T}_{device} \times \frac{q}{4k_b T} \quad (10.2)$$

As in the 2d-2d_{face} case the tunneling only occurs at a single energy due to the conservation of momentum and energy as shown in Fig. 11(e). Since we are now dealing with 1d nanowires, the



number of transverse states follows a 1d density of states which follows a $1/\sqrt{V_{OL}}$ dependence. This is illustrated in Fig. 11(d). This predicts a step function turn on followed by a reciprocal square root decrease. This seemingly implies that the initial conductance will be infinite. However, the contact series resistance will limit the conductance and the broadening associated with the contacts will also limit the peak conductance.

XI. Perturbation Tunnel Transmission Limit

When a level on the p-side of a junction interacts with a level on the n-side of the junction it is possible for the two levels to interact strongly and repel each other. In most cases this is not a problem, as the interaction between any two *particular* levels goes to zero as the devices get larger and any small amount of level broadening will wash out the level repulsion. In the case of very large contact regions leading to the tunnel junction, the large normalization volume of the wave functions guarantees that individual level repulsion matrix elements are negligible.

In contrast, the 0d-0d, 1d-1d edge overlap and 2d-2d area overlap cases, have finite extent along the tunneling direction, restricting the normalization volume. This means that the tunnel interaction matrix element, $|M_{fi}|$, can take on a large finite value. If this interaction is too large, the two interacting levels will be strongly coupled and all the perturbation results in this paper will fail. Contrarily, if the level broadening is greater than the level repulsion matrix element, $\gamma > |M_{fi}|$, the level repulsion will be washed out justifying our perturbation approach. The broadening γ is typically caused by coupling to the contacts.

We will show that if the current is limited by the weak tunneling junction rather than the contact resistances, we will have $|M_{fi}| < \gamma$, and the levels will be sufficiently broadened for

perturbation theory. This will occur if the allowed contact current is greater than device current which is limited by tunneling transmission $\mathcal{T}_{\text{device}}$. For a single level device such as the 0d-0d and 1d-1d_{edge}, the contact current can be related²⁰ to the broadening γ to give: $I_{\text{contact}}=2q\gamma/\hbar$, from Section VII, where the factor 2 is due to spin. The device current is given by Fermi's golden rule:

$$I_{\text{device}} = 2q \times \frac{2\pi}{\hbar} \times |M_{fi}|^2 \times \frac{dN}{dE} \quad (11.1)$$

The density of states dN/dE can also be expressed as the inverse of the level spacing, ΔE : $dN/dE=1/\Delta E$ if $\Delta E < \gamma$, or $dN/dE=1/\gamma$ if $\Delta E > \gamma$. Using this and setting $I_{\text{device}} < I_{\text{contact}}$ gives $|M_{fi}|^2 < (\gamma \times \Delta E)$ or $|M_{fi}|^2 < \gamma^2$, respectively. But in the first case $\Delta E < \gamma$ assures $|M_{fi}| < \gamma$. Therefore in both cases $|M_{fi}| < \gamma$ satisfies the level broadening requirements for Fermi's Golden Rule, and limits the permitted tunneling current.

Perturbation theory requires the matrix element to be less than the width of the broadening. We have shown that the levels are sufficiently broadened when the device current is limited by the tunneling junction but not limited by the contacts. The same restriction on tunnel junction current applies to the 2d-2d_{face} case, since both the contact current and the device current are multiplied by the number of transverse y states and can be analyzed as many 1d-1d_{edge} modes in parallel.

The tunneling matrix element, which is less than γ , is given by Eq'n. (A.12):

$$|M_{fi}| = \frac{1}{\pi} \sqrt{E_{Z,i} \times E_{Z,f} \times \mathcal{T}_{\text{device}}}. \quad \text{Solving for the maximum permitted tunneling transmission}$$

probability $\mathcal{T}_{\text{device}}$ in the general case:

$$\mathcal{T}_{\text{device}} < \frac{\pi^2 \gamma^2}{E_{Z,i} \times E_{Z,f}} \quad (11.2)$$

This perturbation requirement applies to the 0d-0d, 1d-1d_{edge}, and 2d-2d_{face} cases.

Now specifically considering the 0d-0d case, the contact broadening is Eq'n. (8.4), $\gamma = (1/\pi) \times E_{Z,i} \times T_{\text{contact}}$. Inserting this into the maximum permitted tunneling transmission probability, Eq'n. (11.3), with the E_Z confinement energies equal, the basic requirement $|M_{fi}| < \gamma$ implies:

$$T_{\text{device}} < T_{\text{contact}}^2 \quad (11.3)$$

which we regard as the condition for the validity of time-dependent perturbation theory for the 0d-0d case.

The contact broadening for a specific 1d-1d_{edge} case will now be worked out:

We consider the 1d-1d_{edge} case with contacts consisting of nanowires extending to infinity. The electrical contact broadening for 1d-1d edge overlapped nanowires, Fig. 11(a), is controlled by the loss of carriers into the extended nanowires. Let the length of the overlap region be L_X . In each wire, the carrier will travel an average distance of L_X before escaping. At turn on, its momentum is given by $p_X = mv_X = \hbar k_X$ where $k_X = \pi/L_X$ in the ground state. Using $E_X = \hbar^2 k_X^2 / 2m = \hbar^2 \pi^2 / 2m L_X^2$, the average escape time is $\tau = L_X / v_X = \hbar / 4E_X$. Then the energy level broadening due to contacts is:

$$\gamma \equiv \hbar / \tau = (2/\pi) E_X = (2/\pi) \hbar^2 \pi^2 / 2m L_X^2 \quad (11.4)$$

The coupling matrix element is the same as the 0d-0d case and is given by Eq'n. (A.12):

$$|M_{fi}| = \frac{1}{\pi} \sqrt{E_{Z,i} \times E_{Z,f} \times T_{\text{device}}}. \text{ Requiring } |M_{fi}| < \gamma \text{ implies that the tunneling transmission factor}$$

T_{device} should not be too large:

$$\sqrt{T_{\text{device}}} < \frac{2L_{Z,i} \times L_{Z,f}}{L_X^2} \quad (11.5)$$

This is the condition for perturbation theory to be valid for 1d-1d_{edge} case contacted by extended wires. The same condition applies to the 2d-2d_{face} case because it can be analyzed as many 1d-1d_{edge} modes in parallel.

XII. Maximum Conductance Limit

Since we have found a maximum permitted tunneling transmission, $\mathcal{T}_{\text{device}}$ for perturbation theory, this sets the maximum permitted current or conductance within our perturbation approach. For the 0d-0d case we already derived Eq'n. (8.10), the conductance $G/(q^2/h) = 2\pi^2\gamma/(k_b T) \times [\mathcal{T}_{\text{device}}/(\mathcal{T}_{\text{contact}})^2]$. The maximum permitted tunneling transmission is $[\mathcal{T}_{\text{device}}/(\mathcal{T}_{\text{contact}})^2] = 1$, which leads to the maximum permitted conductance:

$$G_{0d-0d} < \frac{2q^2}{h} \times \pi^2 \times \frac{\gamma}{k_b T} \quad (12.1)$$

which is unfortunately less than the conductance quantum for sharp thresholds, $\gamma < k_B T$.

For the 1d-1d_{edge} case the expression for the 1d-1d_{edge} conductance is Eq'n. (10.2):

$$G_{1d-1d, \text{edge}} = 2 \frac{L_x}{\pi^2 \hbar^2} E_{Z,i} \times E_{Z,f} \times \sqrt{\frac{m}{qV_{OL}}} \times \mathcal{T}_{\text{device}} \times \frac{q}{4k_b T}$$

In the most general damping model $\gamma > |M_{fi}| = \frac{1}{\pi} \sqrt{E_{Z,i} \times E_{Z,f} \times \mathcal{T}_{\text{device}}}$. Plugging $|M_{fi}| = \gamma$ into

$G_{1d-1d, \text{edge}}$ and setting $qV_{OL} = \gamma$ to provide the peak permitted conductance gives:

$$G_{1d-1d, \text{edge}} < \frac{2q^2}{h} \times \sqrt{2}\pi^2 \times \gamma^{3/2} \times \frac{1}{4k_b T} \times \sqrt{\frac{2mL_x^2}{\pi^2 \hbar^2}} \quad (12.2)$$

Now we specialize to damping due to extended nanowire contacts reaching to infinity. Inserting the broadening equation, Eq'n. (11.4), $\gamma = (2/\pi)E_x$, and the explicit expression $E_x = \hbar^2 \pi^2 / 2mL_x^2$ gives the maximum conductance:

$$G_{1d-1d,edge} < \frac{2q^2}{h} \times \frac{\pi^{3/2}}{2} \times \frac{\gamma}{k_b T} \quad (12.3)$$

which is a similar limit as the 0d-0d case.

The derivation for the 2d-2d_{face} case maximum permitted conductance is similar:

From Eq'n. (9.3):

$$G_{2d-2d,face} = \frac{qmA}{\pi^2 \hbar^3} \times E_{Z,i} \times E_{Z,f} \times \mathcal{T}_{device} \times \frac{q}{4k_b T}$$

Where $A \equiv W \times L_X$ is the area of the overlap region between quantum wells. Once again, in the

most general damping model $\gamma = |M_{fi}| = \frac{1}{\pi} \sqrt{E_{Z,i} \times E_{Z,f} \times \mathcal{T}_{device}}$. Plugging $|M_{fi}| = \gamma$ into $G_{2d-2d, face}$,

we obtain the general maximum permitted conductance:

$$G_{2d-2d,face} < \frac{2q^2}{h} \times \frac{\pi^3}{2} \times \gamma^2 \times \frac{1}{4k_b T} \times \left(\frac{2mWL_X}{\hbar^2 \pi^2} \right) \quad (12.4)$$

Now we specialize to damping owing to extended quantum well contacts reaching to infinity. Inserting the broadening equation, Eq'n. (11.4), $\gamma = (2/\pi)E_X$, and the explicit expression

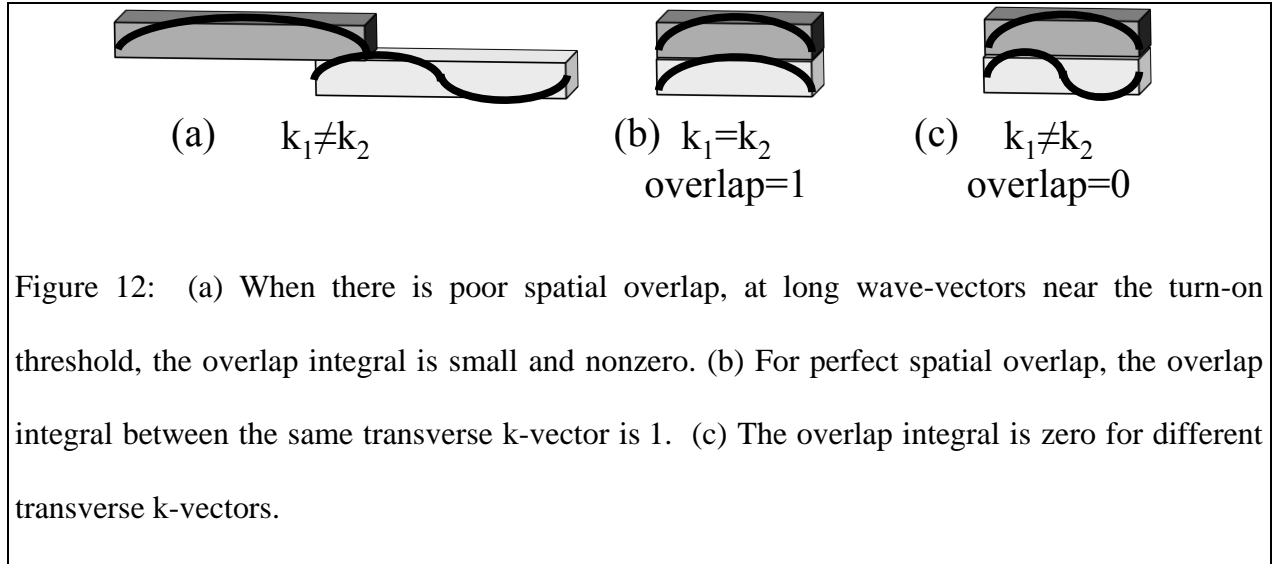
$E_X = \hbar^2 \pi^2 / 2mL_X^2$ gives the maximum conductance:

$$G_{2d-2d,face} < \frac{2q^2}{h} \times \frac{\pi^2}{4} \times \frac{\gamma}{k_b T} \times \frac{W}{L_X} \quad (12.5)$$

Thus we have obtained the maximum permitted perturbation conductance for the 0d-0d, 1d-1d, and 2d-2d cases, for both general damping and for end-wire damping models. Within the limits of perturbation theory all of the cases have a tradeoff between the broadening and the conductance.

XIII. Smearing the Steep Response:

The finite overlap length L_X of the 1d-1d_{edge}, and 2d-2d_{face} cases led to loss of carriers to the extended nano-wire/quantum well contacts, and the damping smeared the steep response. We can show the modification of the steep response in an entirely different way, by employing the exact wave functions at the ends of the wires. The wave-functions are illustrated in Fig. 12(a) where long wavelengths approach zero at the ends of the wires, precisely where overlap is needed. These long wavelengths occur right at threshold, impairing the sharp turnon.



On the other hand, shorter wavelengths as shown 12(b) and 12(c) are either overlapping in Fig. 12(b) or orthogonal in Fig. 12(c). If there is a perfect overlap the states completely couple by tunneling.

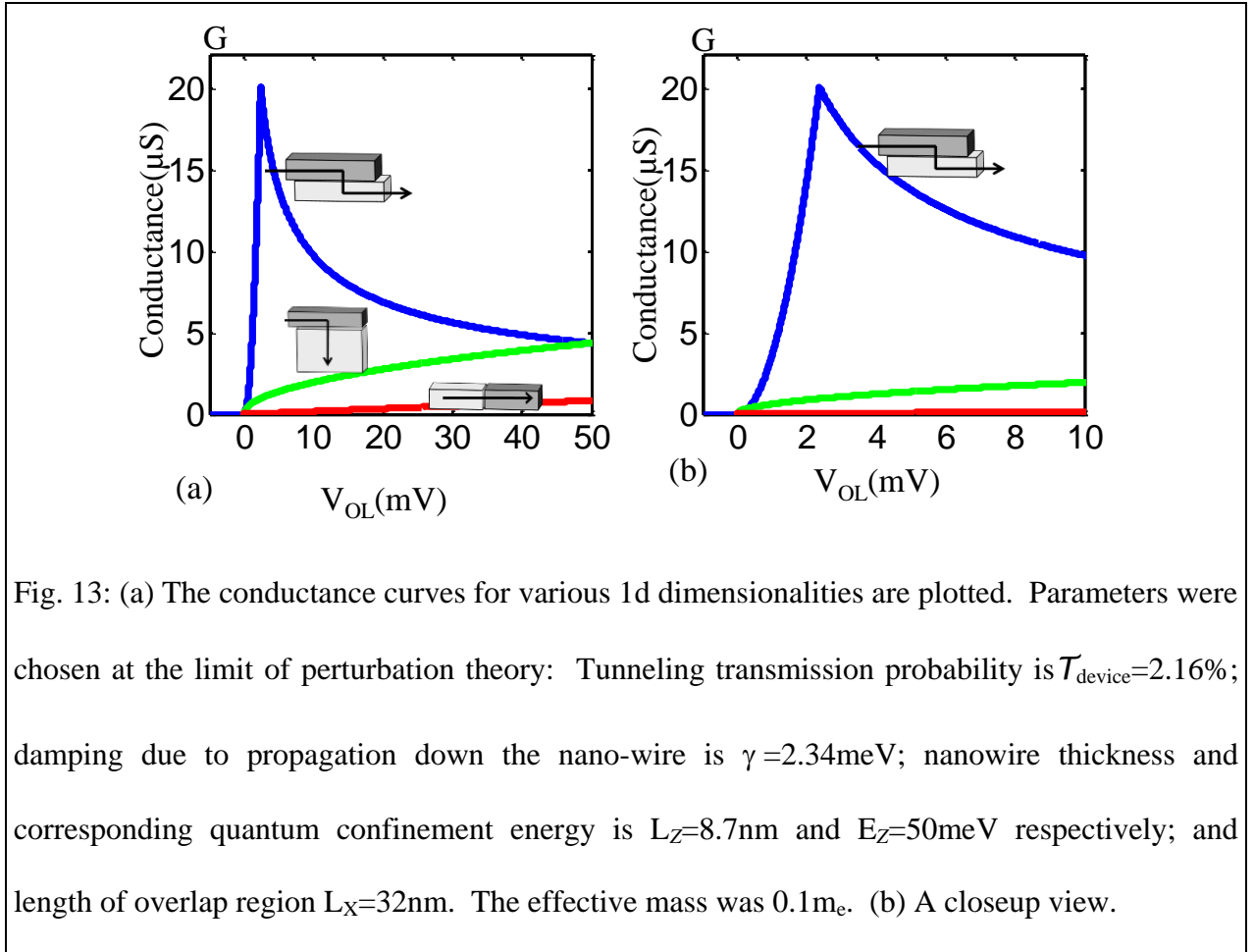
The shape of the turn on due to wave functions going to zero at the wire ends can be modeled following the methods in the Appendix. The kronecker deltas in Eq'n. (A.10) need to be replaced by the actual transverse overlap integral from Eq'n. (A.5) and the sums in Eq'n. (B.4) should include all the transverse states. Taking the limit near turnon for long k-vectors, we get the following expressions for the conductivities:

$$G_{1d-1d_{edge}, \text{tum-on}} \approx \frac{2q^3}{h} \times \frac{\pi^5}{72} \times \frac{E_{Z,i} E_{Z,f}}{E_X^3} \times V_{OL}^2 \times \mathcal{T}_{\text{device}} \times \frac{q}{4k_b T} \quad (13.1)$$

$$G_{2d-2d_{face}, \text{tum-on}} \approx \left(\frac{2q^3}{h} \times \frac{\pi^5}{72} \times \frac{E_{Z,i} E_{Z,i}}{E_X^3} \times V_{OL}^2 \times \mathcal{T}_{\text{device}} \times \frac{q}{4k_b T} \right) \times \frac{14}{15} \times \frac{W}{\pi \hbar} \sqrt{\frac{qmV_{OL}}{2}} \quad (13.2)$$

where, W is the width of the quantum well. The turn-on conductance versus overlap control voltage V_{OL} can be seen in Fig. 13 for the 1d-1d_{edge}, 1d-2d, and 1d-1d_{point} cases. Similarly Fig. 14 covers the 2d-2d_{face}, 2d-3d, 3d-3d and 2d-2d_{edge} cases, with conductance per unit width plotted.

The effective broadening is the overlap voltage required to reach peak conductance for the 1d-1d_{edge} and 2d-2d_{face} cases that would otherwise have been infinitely sharp.



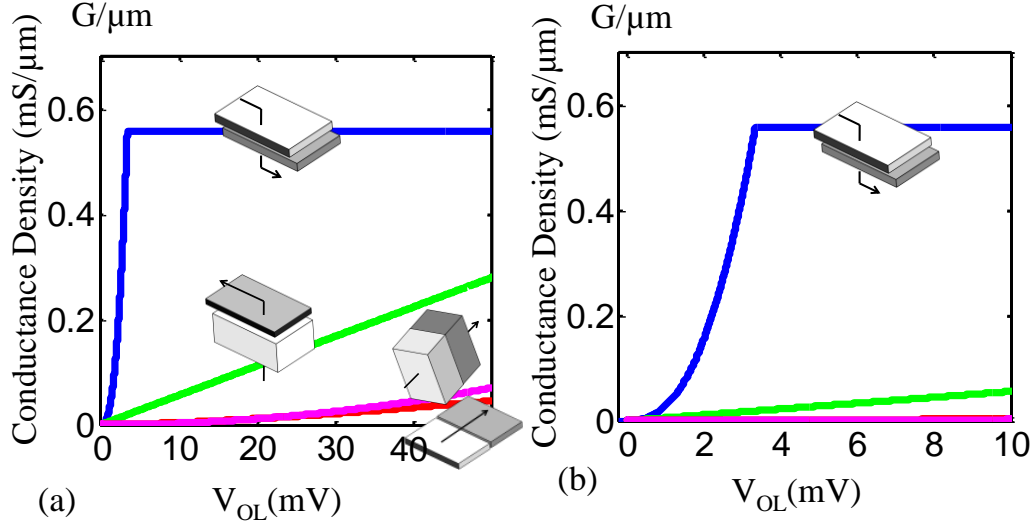


Fig. 14: (a) The conductance curves for various 2d and 3d dimensionalities are plotted. The parameters chosen were the same as in Fig. 13, at the limit of perturbation theory: Tunneling transmission probability is $T_{\text{device}}=2.16\%$; damping due to propagation down the nano-wire is $\gamma=2.34\text{meV}$; nanowire thickness and corresponding quantum confinement energy is $L_Z=8.7\text{nm}$ and $E_Z=50\text{meV}$ respectively; and length of overlap region $L_X=32\text{nm}$. The effective mass was $0.1m_e$. (b) A closeup view.

For the 1d-1d_{edge} case, the voltage requirement is met when Eq'n. (13.1) equals the on

state conductance Eq'n. (10.2): $G_{1d-1d,\text{edge}} = 2 \frac{Lq}{\pi^2 \hbar^2} E_{Z,i} \times E_{Z,f} \times \sqrt{\frac{m}{qV_{OL}}} \times T_{\text{device}} \times \frac{q}{4k_b T}$. This

gives an effective broadening:

$$\gamma \equiv qV_{OL} = \left(\frac{72\sqrt{2}}{\pi^5} \right)^{\frac{2}{3}} E_X = 0.48 E_X \quad (13.3)$$

Likewise for the 2d-2d case the voltage requirement is met when Eq'n. (13.2) equals the on state conductance Eq'n. (9.3) $G_{2d-2d,face} = \frac{qmA}{\pi^2 \hbar^3} \times E_{Z,i} \times E_{Z,f} \times T_{device} \times \frac{q}{4k_b T}$. This gives an effective broadening:

$$\gamma \equiv qV_{OL} = \left(\frac{540}{7\pi^4} \right)^{\frac{2}{5}} E_X = 0.91 E_X \quad (13.4)$$

In both cases $\gamma \sim E_X$ which is what we found in the simple escape time model given by Eq'n. (11.4).

XIV. Density of States Broadening

In sections I to X we have assumed an ideal 1d, 2d or 3d density of states and ignored any level broadening. In practical devices the band edges will not have an ideal density of states that fall sharply to zero at the band edge, but rather there will be a band tail. This tail will be caused by any imperfections in the lattice, whether they are due to impurities or phonons. In optical measurements this results in the Urbach tail of the absorption spectrum. In silicon the optical absorption coefficient falls off as an exponential at the rate of 23mV/decade^{23,24}. If a similar tail exists in tunneling devices it could also pose a limit on the achievable sub-threshold slope.

XV. Conclusions

Since there were many geometries, and many different cases covered here, we provide a global Table I that covers all the cases considered in this paper.

Dimensionality significantly affects the low voltage turn on characteristics of a tunneling device, including Backward Diodes and tunneling Field Effect Transistors. The ideal tunneling transistor would have step function turn on characteristic. Fortunately, a 2d-2d_{face} overlapped

tunneling junction is very close to this. In practice, various effects such as nonuniformities, dopants, phonons, series resistance, level broadening, poor wavefunction overlap, will prevent us from observing an ideal 2d density of states step function turn on. In spite of non-idealities the 2d-2d_{face} overlapped junction is expected to bring us closer to a step function response. Furthermore quantum confinement on either side of a tunneling barrier can significantly boost the on-state conductance.

XVI. Acknowledgment

This work was supported by the Center for Energy Efficient Electronics Sciences, which receives support from the National Science Foundation (NSF award number ECCS-0939514).

Case	Picture	Current	Conductance, G	Maximum G for pert. theory to be valid	Maximum G for end contacts $\gamma = (2/\pi)E_x$
1d-1d		$\frac{2q^2}{h} \times V_{OL} \times T_{device}$	$\frac{2q^2}{h} \times V_{OL} \times T_{device} \times \frac{q}{4k_b T}$	N/A	N/A
3d-3d		$\frac{Am^*}{4\pi\hbar^2} \times \frac{qV_{OL}}{2} \times \frac{2q^2}{h} V_{OL} \times T_{device}$	$\frac{Am^*}{4\pi\hbar^2} \times \frac{qV_{OL}}{2} \times \frac{2q^2}{h} V_{OL} \times T_{device} \times \frac{q}{4k_b T}$	N/A	N/A
2d-2d _{edge}		$\frac{2L_X \sqrt{qm^*} V_{OL}}{3\pi\hbar} \times \frac{2q^2}{h} \times V_{OL} \times T_{device}$	$\frac{2L_X \sqrt{qm^*} V_{OL}}{3\pi\hbar} \times \frac{2q^2}{h} \times V_{OL} \times T_{device} \times \frac{q}{4k_b T}$	N/A	N/A
0d-1d		$\frac{2q}{h} \times E_Z \times T_{device}$	$\frac{2q}{h} \times E_Z \times T_{device} \times \frac{q}{4k_b T}$	N/A	N/A
2d-3d		$\frac{Am}{2\pi\hbar^2} \times \frac{qV_{OL}}{2} \times \frac{4q}{h} \times E_Z \times T_{device}$	$\frac{Am}{2\pi\hbar^2} \times \frac{qV_{OL}}{2} \times \frac{4q}{h} \times E_Z \times T_{device} \times \frac{q}{4k_b T}$	N/A	N/A
1d-2d		$\frac{L_X}{\pi\hbar} \times \sqrt{qm^*} V_{OL} \times \frac{4q}{h} \times E_Z \times T_{device}$	$\frac{L_X}{\pi\hbar} \times \sqrt{qm^*} V_{OL} \times \frac{4q}{h} \times E_Z \times T_{device} \times \frac{q}{4k_b T}$	N/A	N/A
0d-0d		$\frac{4q}{h} E_{Z,i} \times \frac{T_{device}}{T_{contact}}$	$\frac{4q}{h} E_{Z,i} \times \frac{T_{device}}{T_{contact}} \times \frac{q}{4k_b T}$	$\frac{2q^2}{h} \times \pi^2 \times \frac{\gamma}{k_b T}$	$\frac{2q^2}{h} \times \pi^2 \times \frac{\gamma}{k_b T}$
2d-2d _{face}		$\frac{qmA}{\pi^2\hbar^3} \times E_{Z,i} \times E_{Z,f} \times T_{device}$	$\frac{qmA}{\pi^2\hbar^3} \times E_{Z,i} \times E_{Z,f} \times T_{device} \times \frac{q}{4k_b T}$	$\frac{2q^2}{h} \times \frac{\pi^3}{2} \times \gamma^2 \times \frac{1}{4k_b T} \times \frac{2mA}{\hbar^2 \pi^2}$	$\frac{2q^2}{h} \times \frac{\pi^2}{4} \times \frac{W}{L_x} \times \frac{\gamma}{k_b T}$
1d-1d _{edge}		$2 \frac{qL_X}{\pi^2\hbar^2} E_{Z,i} \times E_{Z,f} \times \sqrt{\frac{m}{qV_{OL}}} \times T_{device}$	$2 \frac{qL_X}{\pi^2\hbar^2} E_{Z,i} \times E_{Z,f} \times \sqrt{\frac{m}{qV_{OL}}} \times T_{device} \times \frac{q}{4k_b T}$	$\frac{2q^2}{h} \times \sqrt{2\pi^2} \times \gamma^{3/2} \times \frac{1}{4k_b T} \times \sqrt{\frac{2mL_x}{\pi^2\hbar^2}}$	$\frac{2q^2}{h} \times \frac{2\pi^{3/2}}{4} \times \frac{\gamma}{k_b T}$

Appendix A: Transfer-Matrix Element Derivation

In our derivation of the tunnel matrix element by the transfer Hamiltonian method we will consider 3d-3d case. The method for the other reduced dimensionality cases is very similar and we will note some of the changes that would be necessary for those cases as we go through the derivation.

First we consider a simple Type III junction band diagram as shown in Fig. 15. The total Hamiltonian H , is illustrated in Fig. 15(a). The incomplete initial Hamiltonian H_i , on the left is in Fig. 15(b), and the incomplete final state Hamiltonian H_f on the right is in Fig. 15(c). For the cases in Figs. 15(b)&(c), the incomplete Hamiltonians lead to their own stationary Schrodinger's equations: $H_i|\Psi_i\rangle=E_i|\Psi_i\rangle$ and $H_f|\Psi_f\rangle=E_f|\Psi_f\rangle$ respectively. The subscript 'i' represents the initial electron in the valence band and the subscript 'f' represents the final electron in the conduction band.

In the true full Hamiltonian, H , a valence band electron on the left decays exponentially into the barrier, and tunnels to the conduction band on the right. The perturbation Hamiltonian with respect to the starting Hamiltonian is therefore $H'=H-H_i$. The Fermi's Golden Rule transition rate for an electron in the valence band on the left, tunneling to the conduction band on the right, is.

$$R_{if} = \frac{2\pi}{\hbar} \left| \langle \Psi_f | H' | \Psi_i \rangle \right|^2 \frac{dN}{dE} = \frac{2\pi}{\hbar} \left| \langle \Psi_f | H - H_i | \Psi_i \rangle \right|^2 \frac{dN}{dE} = \frac{2\pi}{\hbar} \left| \langle \Psi_f | H - E_i | \Psi_i \rangle \right|^2 \frac{dN}{dE} \quad (A.1)$$

where we used the fact that $H_i|\Psi_i\rangle=E_i|\Psi_i\rangle$, and dN/dE represents the density of final states.

The exact Hamiltonian, in Fig. 15(a) naturally divides into three regions. For $z < 0$ the system resembles H_i , whose eigenstates are in the valence band on the left. For $0 < z < L$, there is a barrier which the electron must tunnel through, and for $z > L$ the system resembles H_f with eigenstates in the conduction band on the right. Ψ_i is a free particle in the valence band and the

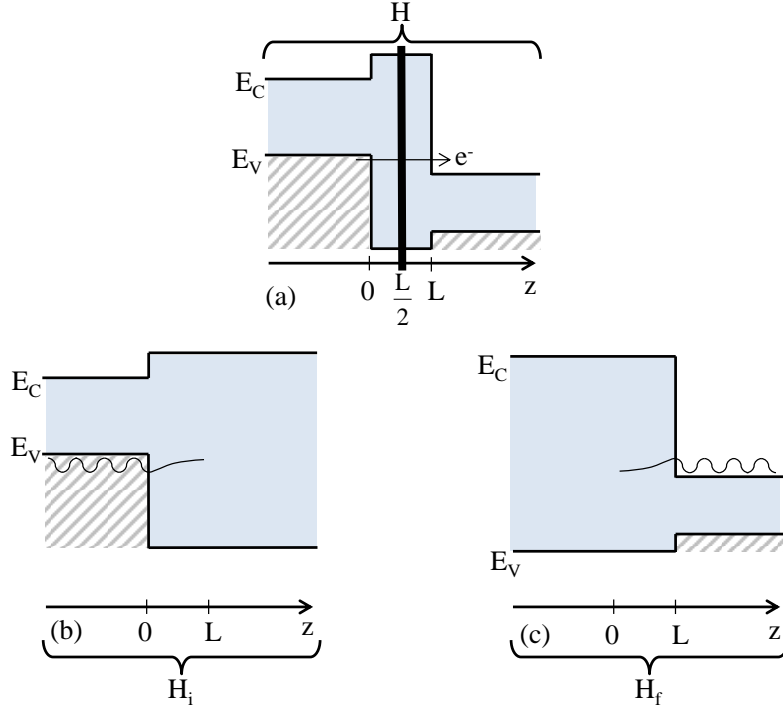


Figure 15: (a) The exact total Hamiltonian H . (b) The incomplete Hamiltonian H_i whose eigenstate represents the initial valence electron of energy E_i . (c); The incomplete Hamiltonian H_f whose eigenstate represents the final conduction band electron of energy E_f .

exponential decay can be modeled by the WKB approximation. For convenience we segregate the problem into halves, picking a surface somewhere in the barrier so that we can divide the junction into a left half and a right half. For simplicity we choose the dividing plane to be at $L/2$ as shown in Fig. 15(a).

Since $(H_i - E_i)|\Psi_i\rangle = 0$ everywhere, and $H \equiv H_i$ in the left half space, then $(H - E_i)|\Psi_i\rangle = 0$, in the left half-space; $z < L/2$. Likewise, since $(H_f - E_f)|\Psi_f\rangle = 0$ everywhere, and $H \equiv H_f$ in the right half-space, then, $(H - E_f)|\Psi_f\rangle = 0$, in the right half-space; $z > L/2$.

Following refs. 14&15, the matrix element, $M_{fi} = \int_{-\infty}^{\infty} d^3r \psi_f^* (H - E_i) \psi_i$ can be simplified by recognizing that the integral is certainly zero for $z < L/2$ and by subtracting

$0 = [\psi_i^* (H - E_f) \psi_f]^*$ for $z > L/2$. Further simplification arises when we express the Hamiltonian in the standard format:

$$H = -\frac{\hbar^2 \nabla^2}{2m} + V(r) \quad (A.2)$$

where $V(r)$ describes the entire potential of the junction. By substituting this into:

$$M_{fi} = \int_{z>L/2}^{\infty} d^3r [\psi_f^* (H - E_i) \psi_i - \psi_i (H - E_f) \psi_f^*] \quad (A.3)$$

and using both energy conservation, $E_i = E_f$, and the cancellation of terms involving $V(r)$, we will be left with:

$$\begin{aligned} M_{fi} &= \frac{-\hbar^2}{2m} \int_{z>L/2} d^3r \times (\psi_f^* \nabla^2 \psi_i - \psi_i \nabla^2 \psi_f^*) \\ &= \frac{-\hbar^2}{2m} \int_{z>L/2} d^3r \times \nabla \cdot (\psi_f^* \nabla \psi_i - \psi_i \nabla \psi_f^*) \end{aligned} \quad (A.4)$$

Now we use Gauss's law to express the matrix element as:

$$M_{fi} = \hbar i \int_{z=L/2} \vec{G}_{fi} \cdot d\vec{S} \text{ where} \quad (A.5)$$

$$\text{with } \vec{G}_{fi} \equiv \frac{i\hbar}{2m} (\psi_f^* \nabla \psi_i - \psi_i \nabla \psi_f^*) \quad (A.6)$$

The matrix element is now expressed as a surface integral of \vec{G}_{fi} which is nonzero only at the $z=L/2$ surface.

To determine the tunneling matrix element (A.5) in our case of 3d-3d bulk tunneling we must first write down Ψ_i and Ψ_f in order to evaluate G_{fi} . Within the effective mass approximation, we can use the WKB approximation to write down the wave functions. We neglect the underlying Bloch functions, but for a more complete treatment see ref. 16. We also assume that most of the probability density is outside of the barrier region and so the barrier

region can be neglected when calculating the normalization constant. The normalized WKB approximation becomes:

$$\psi_i = \sqrt{\frac{2k_{z,i}}{L_X L_Y L_{z,i}}} \times \exp(ik_{x,i}x + ik_{y,i}y) \times \frac{1}{\sqrt{k_z(z)}} \times \begin{cases} \sin\left(\int_z^0 k(z') \times dz' + \frac{\pi}{4}\right), & z < 0 \\ \frac{1}{2} \exp\left(-\int_0^z k(z') \times dz'\right), & z \geq 0 \end{cases} \quad (\text{A.7a})$$

$$\psi_f = \sqrt{\frac{2k_{z,f}}{L_X L_Y L_{z,f}}} \times \exp(ik_{x,f}x + ik_{y,f}y) \times \frac{1}{\sqrt{k_z(z)}} \times \begin{cases} \sin\left(\int_L^z k(z') \times dz' + \frac{\pi}{4}\right), & z > L \\ \frac{1}{2} \exp\left(-\int_z^L k(z') \times dz'\right), & z \leq L \end{cases} \quad (\text{A.7b})$$

In these equations $k_{\alpha,i}$ and $k_{\alpha,f}$ are the α -component of the k -vector in the initial and final states respectively. $k_z(z)$ is the spatially dependent value of k_z that varies within the barrier. L_X , L_Y , $L_{z,i}$, and $L_{z,f}$ are the dimensions of the device as shown in Fig. 4(a). $L_{z,i}$ represents the length of the left half of the device for $z < 0$. $L_{z,f}$ represents the length of the right half of the device for $z > L$. Plugging these wavefunctions into \vec{G}_{fi} and evaluating it at $z=L/2$ gives:

$$G_{fi,\hat{z}} = -\sqrt{\frac{k_{z,f}k_{z,i}}{L_{z,f}L_{z,i}}} \frac{i\hbar}{2mL_X L_Y} \exp(i\Delta k_X x + i\Delta k_Y y) \times \exp\left(-\int_0^L k_z dz\right) \quad (\text{A.8})$$

where $\Delta k_X = (k_{X,i} - k_{X,f})$ and $\Delta k_Y = (k_{Y,i} - k_{Y,f})$. Using this and evaluating the expression for the matrix element we get:

$$M_{fi} = \frac{\hbar^2}{2m} \sqrt{\frac{k_{z,f}k_{z,i}}{L_{z,f}L_{z,i}}} \times \exp\left(-\int_0^L k_z dz\right) \times \delta_{k_{X,i},k_{X,f}} \delta_{k_{Y,i},k_{Y,f}} \quad (\text{A.9})$$

The kronecker deltas represent the conservation of transverse momentum and show that the conservation is a natural result of calculating the matrix element. For the case of incomplete conservation of momentum, the kronecker deltas will be replaced by the actual surface integral

in Eq'n. (A.4). At this point we desire to replace $\exp\left(-2\int_0^L k_z dz\right)$ with $\mathcal{T}_{\text{device}}$. But we redefine

$\mathcal{T}_{\text{device}}$ to be a phenomenological factor that includes both the WKB exponential and the effect of the underlying Bloch functions. Thus the matrix element is given by:

$$M_{fi} = \frac{\hbar^2}{2m} \sqrt{\frac{k_{z,f} k_{z,i}}{L_{z,f} L_{z,i}}} \times \sqrt{\mathcal{T}_{\text{device}}} \times \delta_{k_{x,i}, k_{x,f}} \delta_{k_{y,i}, k_{y,f}} \quad (\text{A.10})$$

Interestingly, this expression is also valid for all of the reduced dimensionality cases, we just need to sum over fewer k-states.

For the reduced dimensionality cases we can use $k_z = \pi/L_z$ and $E_z = \hbar^2 k_z^2 / 2m^*$ to further simplify the matrix element. For 0d-1d we get the following matrix element:

$$M_{fi,0d-1d} = \sqrt{\frac{E_{z,i}}{\pi} \times \left(\frac{\hbar^2 k_{z,f}}{2m L_{z,f}} \right) \times \mathcal{T}_{\text{device}}} \quad (\text{A.11})$$

For 0d-0d both sides of the junction are confined which gives:

$$M_{fi,0d-0d} = \frac{1}{\pi} \sqrt{E_{z,i} \times E_{z,f} \times \mathcal{T}_{\text{device}}} \quad (\text{A.12})$$

Appendix B: Using the Transfer Matrix Element to Derive Current

In Appendix A we found the matrix element that can be used with Fermi's golden rule. Using this, we can now find the current in any of the different cases. To aid in correctly counting the number of states, we use the delta function version of Fermi's golden rule. The transition rate between two states is:

$$R_{if} = \frac{2\pi}{\hbar} \left| \langle \psi_f | H - E_i | \psi_i \rangle \right|^2 \delta(E_i - E_f) \quad (\text{B.1})$$

We convert the transition rate to a tunneling current by multiplying the rate by the electron charge, summing over initial and final states, and multiplying by the Fermi-Dirac occupation probabilities.

$$J_{\text{Tunnel}} = 2q \sum_{k_i, k_f} R_{if} f_V (1 - f_C) - R_{fi} f_C (1 - f_V) \quad (\text{B.2a})$$

$$= 2q \sum_{k_i, k_f} R_{fi} (f_C - f_V) \quad (\text{B.2b})$$

$$= \frac{4\pi q}{\hbar} \sum_{k_i, k_f} |M_{fi}|^2 \delta(E_C - E_V) (f_C - f_V) \quad (\text{B.2c})$$

Where

$$f_V = \frac{1}{\exp[(E_i - F_p)/k_b T] + 1} \quad (\text{B.3a})$$

$$f_C = \frac{1}{\exp[(E_f - F_n)/k_b T] + 1} \quad (\text{B.3b})$$

F_n and F_p are the quasi Fermi levels for electrons and holes respectively.

Plugging the matrix element Eq'n. A.10 into Eq'n. B.2c for tunneling current gives:

$$I_{\text{Tunnel}} = \frac{\pi q \hbar^3}{m^2} \sum_{k_i, k_f} \frac{k_{Z,i} k_{Z,f}}{L_{Z,i} L_{Z,f}} (f_C - f_V) \times \mathcal{T}_{\text{device}} \times \delta_{k_{X,i}, k_{X,f}} \delta_{k_{Y,i}, k_{Y,f}} \delta(E_i - E_f) \quad (\text{B.4a})$$

$$I_{\text{Tunnel}} = \frac{8q}{h} \sum_{k_i, k_f} \left(\frac{\hbar^2 k_{Z,i}}{2m} \frac{\pi}{L_{Z,i}} \right) \times \left(\frac{\hbar^2 k_{Z,f}}{2m} \frac{\pi}{L_{Z,f}} \right) \times (f_C - f_V) \times \mathcal{T}_{\text{device}} \times \delta_{k_{X,i}, k_{X,f}} \delta_{k_{Y,i}, k_{Y,f}} \delta(E_i - E_f) \quad (\text{B.4b})$$

Interestingly, this expression is also valid for all of the reduced dimensionality cases, we just need to sum over fewer k-states.

For 3d to 3d bulk we break the sums up into a transverse (k_t) and z component (k_z) and then we convert the sums over k_z and k_t to integrals over the z-component of energy (E_Z) and

transverse energy (E_t) respectively. We can then convert the integrals over E_z to integrals over total energy by a change of variables. Subsequently evaluating the delta functions gives us:

$$I_{\text{Tunnel}} = \frac{qmA}{2\pi^2\hbar^3} \int_0^{V_{\text{OL}}} dE_i \int_0^{\min(E, V_{\text{OL}}-E)} dE_t (f_C - f_V) \times \mathcal{T}_{\text{device}} \quad (\text{B.5})$$

Here we take the zero of energy to be at the conduction band edge on the n-side. The transverse energy can be no more than the total energy on either side of the junction. For reduced dimensionalities we will be summing over fewer k-states and so there may be only one or even no integrals.

Now we can set $(f_C - f_V) \approx qV_{\text{SD}}/(4k_B T)$ by assuming small biases less than $k_B T$.

Finally, we evaluate the integrals and divide by V_{SD} to recover Eq'n. (3.3)

$$G_{3\text{d}-3\text{d}} = \frac{1}{2} \left(\frac{Am^*}{2\pi\hbar^2} \times \frac{qV_{\text{OL}}}{2} \right) \times \frac{2q^2}{h} V_{\text{OL}} \times \mathcal{T}_{\text{device}} \times \frac{q}{4k_b T} \quad (\text{B.6})$$

Thus we have finally recovered the equation for 3d-3d bulk tunneling current with small biases.

Next, we consider the 2d-3d case to demonstrate the general applicability of Eq'n. (B.4).

In this case we sum over the transverse states (k_t) and only the final k_z states. After converting the sums to energy integrals and evaluating the delta function we get:

$$I_{2\text{d}-3\text{d}} = \frac{Am}{2\pi\hbar^2} \times \frac{4q}{h} \times \int_0^{\min(E, V_{\text{OL}}-E)} dE_t (f_C - f_V) \times \mathcal{T}_{\text{device}} \quad (\text{B.7})$$

Taking the small bias limit and dividing by V_{SD} we recover Eq'n. (6.2)

$$G_{2\text{d}-3\text{d}} = \left(\frac{Am}{2\pi\hbar^2} \times \frac{qV_{\text{OL}}}{2} \right) \times \left(\frac{4q}{h} \times E_z \times \mathcal{T} \right) \times \left(\frac{q}{4k_b T} \right) \quad (\text{B.8})$$

Similarly, we can derive the current for any of the cases using Eq'n. (B.4).

REFERENCES:

1. *The International Technology Roadmap for Semiconductors (ITRS)*, Available at <http://www.itrs.net/>, (2010)
2. S. H. Kim, et al., "Germanium-Source Tunnel Field Effect Transistors with Record High ION//IOFF," in *2009 Symposium on VLSI Technology*, Kyoto, Japan, pp. 178-179, (2009)
3. W. Y. Choi, et al., "Tunneling Field-Effect Transistors (Tfets) With Subthreshold Swing (SS) Less Than 60 mV/dec," *IEEE Electron Device Letters*, vol. 28, pp. 743-745, (2007).
4. K. Jeon, et al., "Si Tunnel Transistors With a Novel Silicided Source and 46mV/dec Swing," in *2010 IEEE Symposium on VLSI Technology*, Honolulu, Hawaii, pp. 121-122, (2010).
5. T. Krishnamohan, et al., "Double-Gate Strained-Ge Heterostructure Tunneling FET (TFET) With Record High Drive Currents and < 60 mV/dec Subthreshold Slope," in *IEDM 2008. IEEE International Electron Devices Meeting*, San Francisco, CA, p. 3, (2008).
6. J. Knoch, et al., "Impact of the Dimensionality On The Performance Of Tunneling FETs: Bulk Versus One-Dimensional Devices," *Solid-State Electronics*, vol. 51, pp. 572-578, (2007).
7. A. C. Seabaugh and Q. Zhang, "Low-Voltage Tunnel Transistors for Beyond CMOS Logic," *Proceedings of the IEEE*, vol. 98, pp. 2095-2110, (2010).
8. S. M. Sze and K. K. Ng, *Physics of semiconductor devices*: Wiley-Interscience, (2007).
9. J. Karlovsky, "Curvature Coefficient of Germanium Tunnel and Backward Diodes," *Solid-State Electronics*, vol. 10, pp. 1109-1111, (1967).
10. J. N. Schulman and D. H. Chow, "Sb-heterostructure interband Backward Diodes," *IEEE Electron Device Letters*, vol. 21, pp. 353-355, (2000).

11. Z. Ze, *et al.*, "Sub-micron Area Heterojunction Backward Diode Millimeter-wave Detectors With 0.18 pW/Hz $1/2$ Noise Equivalent Power," *IEEE Microwave and Wireless Components Letters*, vol. 21, pp. 267-269, (2011).
12. J. Appenzeller, *et al.*, "Band-to-Band Tunneling In Carbon Nanotube Field-Effect Transistors," *Physical Review Letters*, vol. 93, p. 4, (2004).
13. E. O. Kane, "Theory of Tunneling," *Journal of Applied Physics*, vol. 32, pp. 83-91, 1961.
14. J. Bardeen, "Tunneling From a Many Particle Point of View," *Physical Review Letters*, vol. 6, pp. 57-59, (1961).
15. C. B. Duke, *Tunneling in Solids*, New York: Academic Press, Inc, (1969).
16. W. A. Harrison, "Tunneling from an independent-particle point of view," *Physical Review*, vol. 123, pp. 85-89, (1961).
17. J. R. Oppenheimer, "Three notes on the quantum theory of aperiodic effects," *Physical Review*, vol. 31, pp. 66-81, (1928).
18. G. Gamow, "Zur Quantentheorie des Atomkernes" *Z. Physik* 51, 204 (1928)
19. M. A. Kastner, "The single-electron transistor," *Reviews of Modern Physics*, vol. 64, p. 849, (1992).
20. S. Datta, *Quantum Transport : Atom to Transistor*. Cambridge, UK: Cambridge University Press, (2005).
21. D. J. Griffiths, *Introduction to Quantum Mechanics*, 2 ed. Upper Saddle River, NJ: Prentice Hall, Inc., (1994).
22. M. Sweeny and J. M. Xu, "Resonant Interband Tunnel-Diodes," *Applied Physics Letters*, vol. 54, pp. 546-548, Feb (1989).

23. G. D. Cody, "Urbach Edge of Crystalline and Amorphous Silicon - A Personal Review," *Journal of Non-Crystalline Solids*, vol. 141, pp. 3-15, (1992).
24. T. Tiedje, *et al.*, "Limiting Efficiency of Silicon Solar Cells," *IEEE Transactions on Electron Devices*, vol. 31, pp. 711-716, (1984).